

# Application of Multifidelity Expected Improvement Algorithms to Aeroelastic Design Optimization

Patrick H. Reisenthel<sup>+</sup>  
*Nielsen Engineering & Research, Inc., Santa Clara, California 95054*

and

Theodore T. Allen<sup>‡</sup>  
*The Ohio State University, Columbus, Ohio 43210*

**An efficient, radial basis function-based extension of multifidelity sequential Kriging optimization was developed. This method, referred to as multifidelity sequential radial basis optimization (MFSRBO) addresses multicriteria optimization involving more than a single type of model representing more than a single discipline, and takes into account both the location in design space and the fidelity of further data acquisition/infills. Several variants of the method are discussed, and their potential assessed for future development. The application of MFSRBO is illustrated on a UAV wing design function integrating information from structural and fluid models.**

## Nomenclature

C	=	Cost
$C_{D,i}$	=	Induced drag coefficient
CDF	=	Cumulative Distribution Function
CDL	=	Cross-Disciplinary Link
$C_L$	=	Lift coefficient
$C_m$	=	Pitching moment coefficient
$d$	=	Design space dimensionality
DOE	=	Design of Experiments
EGO	=	Efficient Global Optimization
EI	=	Expected Improvement
$f$	=	Function
HF	=	High-Fidelity
KRG	=	Kriging-based regression
LER	=	Leading Edge Radius
LF	=	Low-Fidelity
LSE	=	Least Squares Estimation
MFSKO	=	Multifidelity Sequential Kriging Optimization
MFSRBO	=	Multifidelity Sequential Radial Basis Optimization
MLS	=	Moving Least Squares
$N[\mu, \sigma]$	=	Random process with normal distribution of mean $\mu$ and standard error $\sigma$
obj	=	Objective function
PRESS	=	Prediction Error Sum of Squares
PRG	=	Polynomial regression
$q_\infty$	=	Freestream dynamic pressure
RBF	=	Radial Basis Function
$s(f)$	=	Standard error of function $f$
SKO	=	Sequential Kriging Optimization
SPSA	=	Simultaneous Perturbation Stochastic Approximation
SRBO	=	Sequential Radial Basis Optimization

<sup>+</sup> Vice President & Chief Scientist, 2700 Augustine Drive, Suite 200, Santa Clara, CA 95054, Senior Member.

<sup>‡</sup> Associate Professor, 1971 Neil Avenue, 210 Baker Systems, Department of ISE, Columbus, OH 43210.

SVD	=	Singular Value Decomposition
SVR	=	Support Vector Regression
TH	=	Maximum structural thickness at a given span location
$\mathbf{x}$	=	Design vector
$\mathbf{X}$	=	Design matrix
$y$	=	Spanwise coordinate
$\mathbf{Y}$	=	Dependent variables data vector
$\hat{\phantom{x}}$	=	Estimated value
*	=	Effective best solution
$\alpha$	=	Angle of attack
$\alpha_o$	=	Root chord angle of attack
$\gamma$	=	Metamodel parameter
$\Lambda$	=	Taper ratio
$\rho$	=	Fluid density
$\sigma_{VM}$	=	von Mises stress
$\theta_o$	=	Root chord maximum structural thickness

## I. Introduction / Motivation

The development of increasingly complex and integrated aerospace vehicles that are capable of a variety of missions is leading engineers and scientists to consider nonconventional airframes, new structural and propulsion concepts and their interactions early in the design cycle. The technical challenges faced in the design of these revolutionary air vehicles range from considerations of extreme environments (e.g., hypersonic or transatmospheric vehicles) to large dynamic shape variations of micro UAVs. This greater range of design options must be examined in cross-disciplinary terms, where design space exploration is needed to reduce uncertainty and increase knowledge to make better decisions. The large dimensionality of such a design space traditionally requires the use of low-fidelity methods at the conceptual design stage, but the need has long been recognized that information from high-fidelity analysis tools should also be incorporated early in the design process, although this brings along certain challenges. Increased computational power and the proliferation of new unmanned aerial vehicle designs have been driving forces in the development of variable fidelity frameworks over the last decade.

Advanced aerospace vehicle design methods must fuse data from multiple sources and various levels of fidelity. Numerous factors need to be considered, including (Ref. 1) spatial resolution, temporal resolution, the physical processes being modeled, the number of objects, number of attributes of each object, and the degree of interaction between these objects.

High-fidelity methods are typically more expensive, and must be used sparingly out of practical necessity. Other factors to consider are that high-fidelity analyses are assumed to be more accurate, but may not always be, and that there are often difficulties related to obtaining good gradients. For example, there might be integer/discrete variables associated with gross topological changes, e.g., number of compressor stages, number of engines, control surfaces, and so on. These amount to major discontinuities (“cliff edges,” in Jarrett’s, Ref. 2, terminology) which computationally efficient gradient-based design optimization methods cannot cross.

An obvious advantage of low-fidelity methods is that they are computationally inexpensive and fast. More rarely mentioned are the potential benefits of low-fidelity methods in a multifidelity framework, namely that they enable effective design exploration, not merely because of their speed, but as an aid to escape noisy local optima due to the nonsmooth nature of the design space, a common occurrence in high-fidelity analyses. The disadvantages of low-fidelity tools are that they may not work for unconventional designs or strongly nonlinear regimes (Ref. 3), or may not be able to produce the quantities of interest (e.g., aerodynamic drag).

A significant issue in multidisciplinary frameworks is the difficulty in specifying consistency between models. A low-fidelity and high-fidelity model are said to be *weakly consistent* if “the projection of the state of the higher resolution model to the space of the lower resolution model is sufficiently close to the state of the low resolution model” (Ref. 1). In many applications, lower fidelity refers to lower resolution, but may also refer to different methodologies involving significant approximations, not only missing detail but also possibly missing key physics (e.g., absence of chemical reactions, aeroelastic/unsteady effects, viscosity, or turbulence).

True integration of the results from codes of varying fidelity poses a number of challenges. One of them is the fact that prediction codes of varying fidelity levels use different input parameterizations and, therefore, operate in different spaces (Refs. 4, 5). Another challenge is the development of effective strategies when low- and high-fidelity models are not consistent, or when weak consistency is satisfied only in a small region of the design space, therefore limiting the efficiency of current multifidelity frameworks and, potentially, the breadth of design options being considered. The question of optimal sampling of the design space, given limited resources, is a critical one

that is fundamentally linked to the characterization of uncertainty and uncertainty requirements. Specifically, there is a need to develop rigorous approaches addressing not only *where* to sample the design space, but also *at what level* of fidelity.

In the past two decades, there have been numerous implementations of variable fidelity ideas based on the concept of “bridge functions” as a re-anchoring framework for correcting low-fidelity analyses in order to approximate the results of high-fidelity analyses. The “beta” factor initially proposed by Chang et al. (Ref. 6) was introduced as a local multiplicative factor, although many researchers (e.g., Refs. 7, 8) have found it advantageous to implement the additive form of the correction. These schemes incorporate Taylor expansion-based corrections between the low- and high-fidelity models, requiring the design space to be smooth, and may require low- and high-fidelity data to be available at the same point. These factors may result in relatively frequent high-fidelity updates and, therefore, only modest improvements in computational savings over conventional optimization. While useful for establishing provable convergence to the high-fidelity optimum, the local correction method has a tendency to limit the step sizes taken in optimization and, more generally, curtails design space exploration.

As pointed out in Forrester et al. (Ref. 9), efficient global optimization revolves around being able to successfully balance exploration and exploitation. Thus, there is a need for a multifidelity framework allowing bold optimization steps. The present work considers both hierarchical<sup>1</sup> and integrated<sup>2</sup> variable-fidelity metamodeling methods whose uncertainty is reduced with each evaluation. In this work, a radial basis function embodiment of these ideas is used to benchmark performance, and illuminate the efficiency potential of multifidelity multidisciplinary optimization.

## II. Objectives

Aerospace finite element method (FEM) and computational fluid dynamics (CFD) simulations continue to increase in fidelity/realism. Yet, even as computer speeds increase, the most realistic models (e.g., of turbulent flows) are still relatively slow computationally, making thorough optimization difficult. In fact, the gap between the computational speed of low-fidelity models and high-fidelity models continues to increase also. As a result, methods for multifidelity optimization which leverage efficient low-fidelity models promise to enable thorough optimization.

In the years following Jones, Schonlau, and Welch (Ref. 10), there has been growing interest in optimization using global metamodels, e.g., Kriging or radial basis functions. Unlike other design of experiments (DOE) methods, like sequential response surface methods, global metamodels can integrate and generate predictions over the entire design space. As a result, they can integrate an entire data set from an entire design optimization process which can involve human participation in the process. Nonglobal metamodeling approaches for multifidelity optimization are described in Singh and Grandhi (Ref. 11). Advances in global metamodeling using radial basis functions can be found in Refs. 12-15. In particular, Žilinskas (Ref. 15) proved the similarity between statistical- and radial basis function-model based global optimization in the presence of noise. In the present work, the radial basis function approach is selected, based on its suitability for use in efficient global optimization and its extension to the multifidelity context (see Section III).

The objectives of the work presented in this paper include (1) developing a multifidelity multidisciplinary framework through alternative formulations to previous methods, and computational and mathematical results, (2) extending Huang et al.'s (Ref. 16) multifidelity design space sampling strategy to manage system updates within integrated and hierarchical global metamodeling approaches, (3) extending the rigorous convergence results from Schonlau (Ref. 17) to multifidelity optimization in the context of radial basis function methods and Kriging models, (4) developing adaptive methods to achieve probabilistic convergence results and enhance performance, and (5) applying the proposed methods to a flying wing-type UAV design function integrating information from structural and fluid models.

## III. Methods

This section describes the methods, assumptions, and procedures used in this work. We begin with an overview of the optimization process, contrasting the traditional approach and the multifidelity framework envisioned in this work. This is followed by a discussion of surrogate models, including the rationale for our choice of radial basis functions. Section V describes the optimization methods, and Section VI documents the computational analyses used in this work.

---

<sup>1</sup> also referred to in this work as “cascading model”

<sup>2</sup> referred to in this work as the “augmented dimensionality model”

## A. Overview

In the conventional view of the design process, decisions evolve over time. At the conceptual design stage and, increasingly, in preliminary design, a large array of options and cross-disciplinary trades are considered, even though the knowledge of the system is necessarily imprecise (Lewis and Mistree, Ref. 18). This is traditionally the *design space exploration* phase, where individual disciplines must be able to challenge the constraints of other disciplines (Holden and Keane, Ref. 19) in order to come up with effective solutions. An outcome of these analyses is, traditionally, to narrow down the design space to smaller, more manageable portions which are subsequently investigated in more detail. The intermediate level of fidelity, though more expensive, is then used to refine the analysis, add geometric detail, and increase the physical fidelity of the models used, thus reducing the uncertainty in the design. Cross-disciplinary interactions are retained in the MDO methods used, but a smaller portion of the design space is considered, to make this tractable in spite of the higher costs. Finally, the detailed design stage is used to further refine the analysis, narrowing the design to a handful of options.

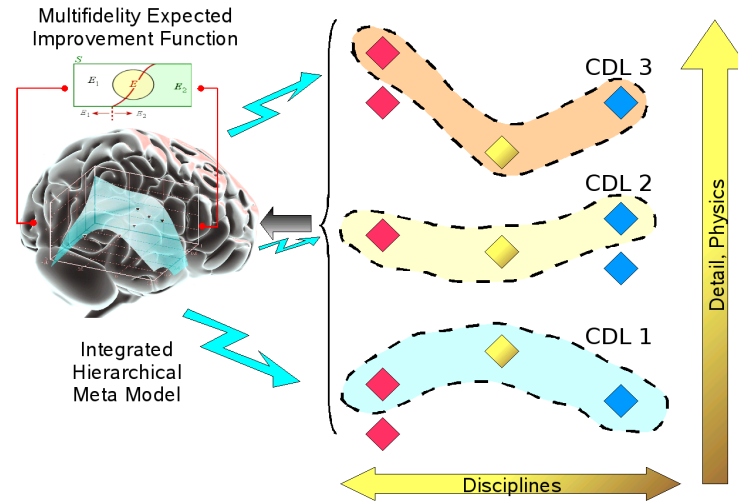


**Figure 1. Multifidelity optimization framework.**

The proposed multifidelity multidisciplinary framework (**Figure 1**) merges information from multiple fidelity levels and manages this information in order to achieve optimal sampling of the design space, both in terms of design variables and level of fidelity. The right-hand side in **Figure 1** represents analysis codes spanning three hypothetical disciplines, e.g., fluids, structures, and guidance and control. Each analysis code is represented by a  $\diamond$  symbol and is ranked according to its level of fidelity, i.e., the level of the physics included in the model and the level of geometric detail. Within the multidisciplinary multifidelity framework, codes with compatible fidelity levels are first coupled together using cross-disciplinary links (CDL). Such groupings are the staple of multidisciplinary optimization (MDO) and include not only the code associations but also the nature of the coupling between them. Within each group, variables appropriately exchanged between disciplines, and the processes for information exchange/update are well-defined. For example, the disciplines within a group can be tightly integrated or loosely coupled, physical interactions accounted for explicitly or through subiterations between codes, and so on.

A key element of the proposed approach is the merging of all multifidelity data into a global probabilistic response surface-based metamodel (see Section IV). This model builds on the foundation provided by multifidelity radial basis function (RBF) data fusion methods (Ref. 20), and optimization methods using probabilistic RBF networks (e.g., Ref. 21). A key addition to these ideas is the use of a Multifidelity Sequential Kriging Optimization (MFSKO)-like “expected improvement function” to manage when high-, medium-, and low-fidelity analysis tools are appropriate as the next observation in the exploration or exploitation of the design space, and associated metamodel updates. The goal of balancing exploration and exploitation in a mathematically rigorous way is achieved by using an integrated criterion which determines simultaneously the location and fidelity level of subsequent searches. This criterion is based on Kennedy and O’Hagan’s original work (Ref. 22), and subsequent refinements by Huang et al. (Ref. 16), and Schenk et al. (Ref. 23).

The work presented in this paper focuses primarily on the multifidelity aspects of aerospace vehicle analysis and design. Thus, the “isofidelity”-groupings depicted in **Figure 1** represent an encapsulation of existing analysis tools, solution methods, and information exchange processes which can operate independently of each other. The central question addressed in this work is how to merge and manage the information from these multiple fidelity groupings.

## B. Background/Rationale

A summary comparing the pros and cons of four different classes of surrogate-based methods is provided in **Table 1**. This summary organizes information gleaned in large part from the review papers of Forrester et al. (Ref. 9) and Queipo et al. (Ref. 24), supplemented with our own experience. The table is organized as follows. The four classes of methods (polynomial, radial basis, Kriging, and support vector regression) are listed across the top. Attributes are listed by row, and are categorized according to (a) forming the metamodel surrogate, (b) optimization considerations, and (c) multifidelity modeling. Whereas many of the table entries are qualitative (e.g., “Low” vs. “Med. Low”), their intent is to give a sense of the relative performance of one method over another. Whenever possible, this sense of performance is quantified in terms of scaling with respect to number of points, search space dimensionality, and so on. Particular method variants may cross boundaries, and not all methods are represented, so this is not intended to be a comprehensive guide but, rather, a reference to help explain where the proposed methods (highlighted) fit within the spectrum of existing approaches.

**Table 1. Suitability Assessment of Surrogate-Based Methods for Multifidelity Multidisciplinary Optimization**

		PRG	MLS	RBF	qParam. RBF	Param. RBF	KRG	Blind KRG	SVR	Param. SVR
Metamodel Construction	Assumption requirements	High	Medium	Med. Low	Low	Low	V. Low	V. Low	Med. Low	V. Low
	Landscape complexity	Low	Medium	Med. High	High	High	V. High	V. High	Med. High	V. High
	Ability to incorporate derivatives	Yes	Yes	Yes	Yes	Yes	Yes	Yes	Unknown	Unknown
	Generalization error	Medium	Low	Med. Low	Low	Low	V. Low	V. Low	Low	V. Low
	Time spent training or retraining the metamodel	Low	High	Low	Low	Medium	High	V. High	V. High	V. High
	Solution effort in terms of number of parameters searched (independently of GCV)*	0	0	0	0	1	2k	2k <sup>2</sup> + 1	2n	2n + 1
	Number of potential regressors, given m data points†	$\frac{(m+d)!}{m!d!}$	$\frac{(m+d)!}{m!d!}$	m	m	m	m	m	m	m
	Maximum number of data points m	High	V. High	< 1000	< 1000	< 1000	< 500	< 500	High	High
	Estimate# of maximum design space dimensionality k	k < 20	k < 20	High	High	High	k < 20	k < 20	High	High
	Ease of implementation	V. High	High	High	High	Medium	Medium	Low	Low	Low
Possibility of error prediction estimates	Yes	Yes	Yes	Yes	Yes	Yes	Yes	Yes	Yes	
Current availability of error estimates	Unknown	Unknown	Yes	Yes	Unknown	Yes	Yes	Yes	Yes	
Optimization	Adaptivity (ability to fit complex local behavior)	Low	Medium	Medium	High	High	High	High	Low	High
	Cost of search	Low	High	Low	Low	Low	Low	Low	Low	Low
	Basic effort associated with a 2-stage infill, in terms of number of parameters searched (independently of GCV)*	0	0	0	0	1	2k	2k <sup>2</sup> + 1	2n	2n + 1
	1-stage# infill effort in terms of number of parameters searched (independently of GCV)*	Unknown	Unknown	k + 1	k + 1	k + 2	3k + 1	2k <sup>2</sup> + k + 1	2n + k + 1	2n + k + 2
	Overall suitability for optimization	Med. Low	Low	Medium	High	High	Med. High	Medium	Low	Low
Suitability for global optimization	V. Low	Low	Medium	High	High	Med. High	Medium	Unknown	Unknown	
Multifidelity	Approximation model or surrogate management framework used	Affine correction process Trust region methods •low level of complexity between fidelity levels •lack of flexibility in terms of point/fidelity selection			•Kennedy - O'Hagan •Dimensionality augmentation + Least Squares Estimation •models complex relationships •flexible point/fidelity selection •fast	Co-Kriging (Kennedy-O'Hagan + Kriging)	•potentially high level of complexity between fidelity levels •flexible point/fidelity selection			Unknown

Notes: \* assumes  $k$ -dimensional design space and  $n$  support vectors  
 † assumes  $m$  data points and polynomial of degree  $d$   
 # (conditional lower bound approach); estimated scaling (except KRG, from Forrester et al., 2009).

# Maximum dimensionality for PRG and MLS limited due to large number of regressors; maximum dimensionality for KRG and Blind KRG limited due to computational effort; potential maximum dimensionality for RBF variants is uncertain, although interpolating RBF solutions of random data in 100+ dimensions have been tested successfully.

It is important to keep in mind that the applicability or optimality of a given method is problem-dependent. A method which may seem unattractive due to its computational demands (e.g., if it involves layer of optimization upon layer of optimization on the surrogate) may still be worth the effort – the answer depends on how costly a single high-fidelity evaluation is. Forrester et al. (Ref. 9) note that, for those very applications, i.e., those most likely to be solved in a highly parallel computing environment, “setting up and searching a surrogate of any kind can (become the) bottleneck. (...) This fact will always limit the amount of time we can dedicate to the building and searching of surrogates.”

In part for this reason, the multifidelity multidisciplinary optimization approach adopted in this work centers on radial basis function (RBF) surrogates, including several of their variants (fixed basis RBF, quasi-parametric RBF, and parametric RBF). As depicted in **Table 1**, this class of methods offers qualities which very nearly approach those of Kriging (in terms of modeling ability, flexibility, and generalization properties) but with potentially significant advantages in terms of performance and scaling. The RBF class of surrogates covers a wide range of methods, from simple fixed basis RBF to fully parametric RBF approaching the complexity of Kriging. Within this class is the freedom to trade generality for performance, depending on which parameters are solved by optimization (parametric RBF) versus which parameters are fixed (RBF). A particularly efficient middle ground is the quasi-

parametric RBF framework, where metaparameters evolve according to a prescribed algorithm. Such algorithms may be rooted in heuristics and are designed to ensure adaptivity while maintaining high performance.

### C. Simple Radial Basis Function Model Description

In an  $N$ -dimensional design space, a surrogate function  $F: \mathbb{R}^N \rightarrow \mathbb{R}$  is constructed by satisfying data constraints at  $P$  available data points. If this response surface acts as an interpolant, then the function  $F$  is required to satisfy the constraints

$$F(\mathbf{X}_i) = Y_i, \quad i = 1, \dots, P \quad (1)$$

where each  $\mathbf{X}_i$  is an  $N$ -dimensional vector of design variables, and  $Y_i$  are the corresponding dependent variables. In the case where  $F$  represents, instead, a regression model fit to the data, then the response surface is required to minimize in the least squares sense the distance  $\|F(\mathbf{X}_i) - Y_i\|$ ,  $i = 1, \dots, M$ ,  $M \geq P$ .

In the radial basis function approach, the metamodel  $F$  is expanded into basis functions  $\Phi_k$  which are radially symmetric about their control point,  $\Gamma_k$ :

$$F(\mathbf{X}) = \sum_k c_k \Phi_k(\mathbf{X}, \Gamma_k, b_k) \quad \Phi_k = f(\|\mathbf{X} - \Gamma_k\|, b_k) \quad (2)$$

where  $f$  is a scalar shape function (for example, a Gaussian),  $b_k$  is an adjustable scale or stiffness parameter, and  $\|\cdot\|$  designates the Euclidean norm. For example, if  $f$  is chosen to be a Gaussian:

$$\Phi_k(\mathbf{X}, \Gamma_k, b_k) = \exp\left(-\frac{(\mathbf{X} - \Gamma_k)^T(\mathbf{X} - \Gamma_k)}{b_k^2}\right) \quad (3)$$

With the additional assumptions that (a) the stiffness  $b_k$  is uniform, and (b) the control points are chosen among the available data points, the linear model regression design matrix equation  $[\mathbf{A}][\mathbf{c}] = [\mathbf{Y}]$  is given by:

$$\begin{bmatrix} f(\|\mathbf{X}_1 - \mathbf{X}_1\|) & f(\|\mathbf{X}_1 - \mathbf{X}_2\|) & \dots & f(\|\mathbf{X}_1 - \mathbf{X}_P\|) \\ f(\|\mathbf{X}_2 - \mathbf{X}_1\|) & f(\|\mathbf{X}_2 - \mathbf{X}_2\|) & \dots & f(\|\mathbf{X}_2 - \mathbf{X}_P\|) \\ \vdots & \vdots & \ddots & \vdots \\ f(\|\mathbf{X}_M - \mathbf{X}_1\|) & f(\|\mathbf{X}_M - \mathbf{X}_2\|) & \dots & f(\|\mathbf{X}_M - \mathbf{X}_P\|) \end{bmatrix} \begin{bmatrix} c_1 \\ c_2 \\ \vdots \\ c_P \end{bmatrix} = \begin{bmatrix} Y_1 \\ Y_2 \\ \vdots \\ Y_M \end{bmatrix} \quad (4)$$

In the case where uncertainty intervals for the  $Y_i$  are available, and provided these intervals correspond to random uncorrelated noise (variance  $\sigma_0^2$ ), the variance of the surrogate prediction at point  $\mathbf{X}$  is given by

$$\hat{\sigma}^2(\mathbf{X}) = \sigma_0^2 \cdot \Phi(\mathbf{X})^T (\mathbf{A}^T \mathbf{A})^{-1} \Phi(\mathbf{X}) \quad (5)$$

where  $\Phi(\mathbf{X}) = [\Phi_1, \Phi_2, \dots, \Phi_P]^T$  (Ref. 25).

## IV. Multifidelity Radial Basis Function Surrogate Models

This section describes multifidelity modeling and discusses its implementation for surrogate models involving radial basis functions. We describe two modeling formulations and variance and bias errors. The first derives from previous research in which radial basis functions model the systematic errors of each surrogate system in relation to higher fidelity systems. The second formulation treats fidelity as a design variable, and adjusts the specific scaling in the radial function.

### A. Modified Kennedy and O'Hagan Scheme

The first and primary modeling formulation is adapted from Kennedy and O'Hagan (Ref. 22) involving both linear and Kriging models. This was the approach used in Huang, Allen, Notz, and Miller (Ref. 26). The ‘‘cascading’’ formulation is:

$$f_l(\mathbf{x}) = f_{l-1}(\mathbf{x}) + \delta_l(\mathbf{x}) \quad (l = 2, 3, \dots, m) \quad (6)$$

where  $f_l$  is the function evaluated at fidelity level  $l$  and  $\delta_l(\mathbf{x})$  is independent of  $f_1(\mathbf{x}), f_2(\mathbf{x}), \dots, f_{l-1}(\mathbf{x})$  and  $\mathbf{x}$  is a  $d$  dimensional decision vector. Hypothetically, different levels of  $l$  also could be different levels of a discrete factor for the same fidelity level. For convenience in the notations below, we also let:

$$f_1(\mathbf{x}) = \delta_1(\mathbf{x}) \quad (7)$$

Note that for  $l = 2, 3, \dots, m$ ,  $\delta_l(\mathbf{x})$  can be understood as the ‘‘systematic error’’ of a lower-fidelity system, ( $l-1$ ), as compared to the next higher-fidelity system,  $l$ . In these cases,  $\delta_l(\mathbf{x})$  is usually small in scale as compared to  $f_l(\mathbf{x})$ , otherwise there will be no reason for the lower-fidelity system to exist. Of course, in some cases, physics may be missed in low-fidelity model(s) and  $\delta_l(\mathbf{x})$  will be large.



$$\mathbf{X} = \begin{bmatrix} \varphi(\mathbf{x}_1, \gamma_1, \mathbf{x}_1, \gamma_1) & \dots & \varphi(\mathbf{x}_1, \gamma_1, \mathbf{x}_n, \gamma_n) \\ \vdots & \ddots & \vdots \\ \varphi(\mathbf{x}_n, \gamma_n, \mathbf{x}_1, \gamma_1) & \dots & \varphi(\mathbf{x}_n, \gamma_n, \mathbf{x}_n, \gamma_n) \end{bmatrix} \quad (13)$$

where it is assumed that all runs have been included in the model as an example. Therefore, Eq. (11) would represent a saturated model that generally passes through all of the design points.

This alternative, more concise formulation has the disadvantage that the  $G_{ij}$  weight parameters must be adjusted heuristically. Also, there is no guarantee that the process will converge to accurate models of the bias or systematic errors or the predictions of the highest fidelity model will converge. Yet, the augmented dimensionality approach includes far fewer parameters to be estimated and can be expected to offer efficiency advantages for cases in which assumption parameters match problem properties closely.

### C. Modeling Prediction Variance

A possible advantage of Kriging models over radial basis functions is that they provide a model of mean and uncertainty even if the model passes through all the design points. Kennedy and O’Hagan (Ref. 22) and others have clarified the Bayesian nature of the intervals. Yet, the interpretation and validity of the derived intervals in realistic cases is not fully understood. At the same time, the computational performance in test problems of methods based on these Kriging error estimates appears to be good.

By contrast, the radial basis functions considered in previous sections are associated with regression type intervals. If the prediction model passes through all the design points, the standard regression intervals indicate zero prediction errors at all points. This follows because the standard intervals are based on so-called variance errors and therefore derive entirely from the assumed repeatability or random errors. We consider four possible approaches to address predictions of prediction uncertainty:

- Assumed random errors – Ad hoc assumptions of random error standard deviation,  $\sigma$ , inserted into the prediction variance formula (similar to Eq. (5)):

$$\hat{\sigma}_l^2(\mathbf{x}) = \text{Var}[y_{\text{prediction}}(\mathbf{x}, l)] = \sigma_0^2 \mathbf{b}(\mathbf{x}, S_1, \dots, S_l)^T (\mathbf{X}' \mathbf{X})^{-1} \mathbf{b}(\mathbf{x}, S_1, \dots, S_l) \quad (14)$$

This approach has some intellectual coherence in the context of FEM. This follows because there is often a known or typical uncertainty associated with computer code, e.g., related to the mesh size. Yet, the errors are not like typical repeatability errors.

- Simply estimated random errors – A selected set of runs can be dropped from the model and used for estimating  $\sigma$ , as is common in regression. In our computational results, we simply drop the most recently collected  $r$  runs from fitting. The standard Analysis of Variance estimate of the random error is then:

$$\hat{\sigma}_0 = \sqrt{[(\mathbf{Y} - \mathbf{X}\boldsymbol{\beta})^T][(\mathbf{Y} - \mathbf{X}\boldsymbol{\beta})]/(n-r)} \quad (15)$$

which is based on an equal variance assumption as is standard in regression.

- PRESS estimated random errors – The standard regression cross validation method of leaving out each observation, fitting with the others, followed by rotating to estimate  $\sigma$ . This estimate is based on an average of calculations from Eq. (15).
- Bias plus variance – Recently developed formulations for the variance and the bias have been developed at OSU which make reference to high-order polynomial true models. The latter offer an intellectually coherent way to assign uncertainty even for cases like FEM with known perfect repeatability. Tseng (Ref. 28) provides several useful formulas.

This last option is in principle the most attractive. However, in practice estimating bias errors requires the assumption of the model form of the true model, e.g., a fourth-order polynomial, and a distribution of the unknown coefficients. The associated arbitrariness of related assumptions makes these methods seem less attractive. Yet, Kriging models have associated ambiguities also relating to the validity and convergence of the assumed correlation parameters. Thus, the present work focuses on the first two options from the above list, leaving the last two options for future research.

## V. Optimization Methods

This section describes the central optimization problem and solution method framework. The framework is based on sequential optimization using radial basis function metamodels. It is based on a search after every computational analysis<sup>3</sup> for the location of the next run in the parameter and fidelity space that maximizes the expected improvement in a manner similar to Huang, Allen, Notz, and Miller (Ref. 16). Next, the expected improvement function is described and method variations based on it are defined.

<sup>3</sup> also referred herein as “experimental run”

### A. The Optimization Problem

Suppose there are a total of  $m$  systems to draw evaluations from, including the real and the surrogates. Denote the output functions of these systems in increasing order of fidelity by  $f_1(\mathbf{x}), f_2(\mathbf{x}), \dots, f_m(\mathbf{x})$ , where  $\mathbf{x}$  is the input vector. Therefore,  $f_1(\mathbf{x})$  has the lowest fidelity, and  $f_m(\mathbf{x})$  has the highest fidelity. As mentioned previously, the highest-fidelity system is the system of interest, therefore the goal is to minimize  $f_m(\mathbf{x})$  within the feasible region,  $\chi$ , i.e.

$$\min_{x \in \chi} f_m(\mathbf{x}) \quad (16)$$

We consider the systems as black boxes that provide no information other than measurements of the outputs. Denoting by  $d$  the dimension of the input space, we assume that the feasible region  $\chi \subset R^d$  is connected and compact.

Each system is associated with a cost-per-evaluation, which is denoted by  $C_1, C_2, \dots, C_m$ , respectively. In this research, the total cost of all evaluations measures the efficiency of the optimization scheme. Usually, a lower-fidelity evaluation is cheaper than a higher-fidelity evaluation, i.e.,  $C_1 < C_2 < \dots < C_m$ . Also, for now we assume that the cost of even the cheapest system is somewhat expensive, such that it is “worthwhile” to regenerate a radial basis function metamodel in order to determine the next search location.

In addition, the measurements of a system output may contain random error or noise. For each system, we assume that random errors from successive measurements are independent identically distributed (IID) normal deviates.

### B. General Optimization Framework

The steps of Multiple Fidelity Sequential Radial Basis Optimization (MFSRBO) are outlined as follows:

- Step 1:** Initialize radial basis function parameter(s), e.g.,  $\gamma$ , and the residual parameters, e.g.,  $r$ , the number of computational analyses for residual or error estimation.
- Step 2:** Perform an initial experimental design involving all fidelity levels. Section C below describes the options and focuses on  $n$  run Latin hypercube initial experiments, following Huang, Allen, Notz, and Miller (Ref. 16).
- Step 3:** Fit the radial basis function of the selected type to all available data using singular value decomposition (SVD)-based least squares estimation.
- Step 4:** Find the location and fidelity level of the new evaluation that maximize the augmented expected improvement (EI) function. If the EI function is sufficiently small, go to Step 6.
- Step 5:** Conduct an evaluation at the selected point from Step 4. Go to Step 3.
- Step 6:** Perform an additional search and/or evaluation to evaluate solution quality. For example, apply trust region evaluation which includes a check for Karush-Kuhn-Tucker point convergence.

Note the removal of a diagnostic step, as compared to the approach used in Ref. 16, because there is no need to assume zero expected mean for the biasing functions,  $\delta_i$ . This constitutes one advantage of sequential radial basis optimization (MFSRBO) methods, which may be expected to lead to relatively robust performance, particularly in cases involving large systematic errors.

By convention, Step 1 is also referred to as the “initial fit” stage, whereas Steps 4 and 5 are called the “infill” or “update” stage. The sequentially added evaluations are also called the “infill” or “update” points. The proposed method differs from its predecessors mainly in the following two aspects: 1) the radial basis function metamodel is generated using multiple fidelity data, and 2) the EI formulation takes into account not only the location but also the fidelity level of an infill point.

### C. Design for Initial Fit

Step 2 in the previous section involves an experimental design for an initial fit. This is essentially the same as the initial step in methods based on Kriging models. Again, assume the number of factors is  $d$ . For the modified Kennedy and O'Hagan scheme, we use an  $n = 10 \times d$  run maximum minimum distance Latin hypercube (from the *lhsdesign* function in MATLAB®) for the lowest fidelity system and then select a subset for higher fidelity systems. If the system includes random errors,  $d$  replicates are added to all levels at locations where the best responses are found.

As another alternative for future exploration, we suggest an initial design that includes all points on a grid for the lowest fidelity level. For each higher fidelity system, a subset of the previous points is selected including the  $q\%$  of the best results from lower fidelity levels. The numerical examples shown here typically use  $q = 25\%$ . The rationale for using a grid instead of a Latin hypercube is that the projection properties of Latin hypercubes are likely not relevant since all systems are generally important. Also, radial basis functions are not affected by the numerical errors for Kriging models associated with equally spaced inputs.

#### D. Expected Improvement Functions

The expected improvement function fits into the search framework and is used to select the next ‘‘infill’’ point. The function balances the desire to improve the search criterion with the desire to reduce uncertainty in a manner reminiscent of trust region point selection. The methods explored here are a straightforward application of the formulation in Huang, Allen, Notz, and Miller (Ref. 16) except that they are based on radial basis functions instead of Kriging models.

Therefore, for Multiple Fidelity Sequential Radial Basis Optimization (MFSRBO), the following augmented Expected Improvement function is proposed:

$$EI(x, l) \equiv E \left[ \max \left( \hat{f}_m(x^*) - \hat{f}_m(x) - \sigma_m(x)\varepsilon, 0 \right) \right] \cdot \alpha_1(x, l) \cdot \alpha_2(x, l) \cdot \alpha_3(l) \quad (17)$$

where  $\varepsilon$  is normally distributed  $N[0,1]$  and

$$\alpha_1(x, l) = \text{function that discounts systems based on their predicted local accuracy,} \quad (18)$$

$$\alpha_2(x, l) = \left( 1 - \hat{\sigma}_0 / \sqrt{\hat{\sigma}_l^2(x) + \hat{\sigma}_0^2} \right), \quad (19)$$

and 
$$\alpha_3(l) = \frac{Cost_m}{Cost_l}.$$

If the problem is deterministic, i.e., with zero repeatability error, then we (generally) use  $\alpha_2(\mathbf{x}, l) = 1$  and  $\hat{f}_m(x^*)$  is the minimum of the already sampled points. More generally, if at least a single system has noise, in Eq. (17),  $\mathbf{x}^*$  stands for the current ‘‘effective best solution’’ defined by

$$x^* = \underset{x \in \{x_1, x_2, \dots, x_n\}}{\operatorname{argmax}} [u(x)] \quad (20)$$

where  $u(x) = -\hat{f}_m(x) - \mu\hat{\sigma}_m(x)$ . The formula from Jones, Schonlau, and Welch (Ref. 10) is:

$$E \left[ \max \left( \hat{f}_m(x^*) - \hat{f}_m(x) - \sigma(x)\varepsilon, 0 \right) \right] = \left( \hat{f}_m(x^*) - \hat{f}_m(x) \right) \Psi \left( \frac{\hat{f}_m(x^*) - \hat{f}_m(x)}{\hat{\sigma}_m(x)} \right) + \hat{\sigma}_m(x) \Phi \left( \frac{\hat{f}_m(x^*) - \hat{f}_m(x)}{\hat{\sigma}_m(x)} \right) \quad (21)$$

where  $\Psi$  is the cumulative normal, and  $\Phi$  is the normal density. We need the two formulas for the variance, i.e., with and without bias. In Ref. 16,  $\alpha_1$  was chosen as

$$\alpha_1(x, l) = \operatorname{corr} \left[ \hat{f}_m(x) + \varepsilon_1 \hat{\sigma}_m(x), \hat{f}_l(x) + \varepsilon_2 \hat{\sigma}_l(x) \right] \quad (22)$$

where ‘‘corr’’ is the correlation function and  $\varepsilon_1$  and  $\varepsilon_2$  are independent normally distributed deviates. This choice has the following desirable properties:

- It is easy to compute in the context of Kriging models,
- When  $l = m$ , it equals 1.
- For deterministic systems, it equals zero at past design points since  $\sigma_l(\mathbf{x})$  is zero.

Unfortunately, for radial basis function systems, Eq. (22) is not easy to compute. In the ‘‘augmented dimensionality’’ version of our method, we inserted an estimate of Eq. (22) based on numerical integration. For other methods, we used the following formulation which is relatively easy to compute:

$$\alpha_1(x, l) = \frac{\hat{\sigma}_l(x)}{|\hat{f}_m(x) - \hat{f}_l(x)| + \hat{\sigma}_m(x)} \quad (23)$$

where  $|\cdot|$  is the absolute value. This approach has the above-mentioned desirable properties in the context of radial basis functions.

#### E. Methods Variations

Every combination of modeling method, expected improvement function (assumed random error, simply estimated random errors, PRESS, and bias plus variance), expected improvement function (deterministic or stochastic), and termination sequence (simple or trust region) hypothetically corresponds to a method variation. Here, we consider only a select few combinations, characteristics of which are summarized in **Table 2**.

If the method has simple termination then it is called multifidelity sequential radial basis optimization (MFSRBO) or, for cases involving only a single level of fidelity, sequential radial basis optimization (SRBO). If the method

terminates by applying a downhill search such as trust region augmented Lagrangian methods, then we refer to the method as a “hybrid.”

**Table 2. Variants considered in the computational and theoretical approach.**

Method Variant	Prediction Uncertainty	EI Function	Termination
1. MFSRBO: augmented dimensionality	Variance Intervals based on assumed prediction errors	Deterministic	Simple
2. MFSRBO: cascading model	Variance intervals from estimated random errors	Deterministic	Simple
3. SRBO: cascading model	Variance intervals from estimated random errors	Stochastic	Simple
4. Hybrid	Variance intervals from estimated random errors	Both	Trust Region Augmented Lagrangian

## VI. Computational Analysis Methods

The computational results presented in this paper consist of several test problems (e.g., Branin function, multifidelity Rosenbrock function) and two applications involving computational structural and computational fluid modeling.

For the structural analysis tool we used McIntosh Structural Dynamics' finite element code CNEVAL (Ref. 29). The wing structure was modeled using conformal quadrilateral plate elements cantilevered at the root chord. Given the normal aerodynamic forces, CNEVAL provides the structural displacements, stresses, frequencies, and overall structural weight. CNEVAL was used to predict the static aeroelastic deformations and to verify that structural limits were not exceeded. CNEVAL uses the current wing planform information, along with thickness distribution and material properties, and updates the finite-element model of the wing, which is subdivided into quadrilateral panels used to distribute the aerodynamic loads for the wing displacement calculations. Each panel is divided into 2 triangles. An option also exists to further subdivide a quad element into 4 triangles for greater accuracy. Both high- and low-fidelity structural modeling were carried out using CNEVAL by changing the finite element discretization, as described in **Table 3**.

**Table 3. Finite element discretization.**

Wing Design Problem	Fidelity Level	Number of Structural Elements		Element Type
		Chordwise	Spanwise	
Unsweped tapered	High	10	15	4 triangle elements per structural quad
	Low	2	2	2 triangle elements per structural quad
UAV, swept	High	10	15	2 triangle elements per structural quad
	Low	4	7	2 triangle elements per structural quad

A version of NEAR's intermediate-level aerodynamic prediction code MISDL (Refs. 30, 31) was used as the high-fidelity fluid model. MISDL is based on panel methods, vortex lattice with compressibility correction for subsonic flow, and other classical singularity methods enhanced with models for nonlinear vortical effects. The method is applicable to subsonic and supersonic flight vehicles including aircraft, UAVs, missiles, and rockets. Circular and noncircular cross section bodies are modeled by either subsonic or supersonic sources/sinks and doublets for volume and angle of attack effects, respectively. Conformal mapping techniques are used for noncircular bodies. The fin/wing sections are modeled by a horseshoe-vortex panel method for subsonic flow and by first-order constant pressure panels for supersonic flow. Up to three lifting surface sections can be modeled, and nonlinear fin and body vortices are modeled. MISDL predicts overall aerodynamic performance coefficients and detailed aerodynamic loading distributions. The code has seen extensive use in missile aerodynamic analysis and design, including aerodynamic shape optimization and multidisciplinary design optimization when coupled to a structural finite element model. In recent years, MISDL has seen use in the analysis of manned and unmanned (UAV) aircraft.

OPTMIS is the name used to designate the version of MISDL that is coupled with CNEVAL. The cross-disciplinary coupling is handled by the OPTMIS logic through successive iteration between codes. OPTMIS handles interpolation, displacement and load transfer operations and iterates between aerodynamic and structural predictions until a prescribed convergence level is achieved. Convergence is reached when the change in the displacements between successive iterations is less than a user-prescribed threshold at all structural node points. For the purposes of this study, OPTMIS was enhanced with the computation of the induced drag. Rather than incorporating a Trefftz plane analysis, such as might be done in an Euler code, the induced drag was computed using a direct method, as follows.

To compute the induced forces on the wing, the Kutta-Joukowski theorem is used:  $\vec{F}_i = \rho \vec{u}_i \times \vec{\Gamma}_i$ . This induced force vector is computed on each panel as the cross product of the total induced velocity on the panel (sum of all vortex lattice induced velocities; the freestream velocity being omitted) and the panel bound vortex vector. The drag component of  $\vec{F}_i$  from each panel is computed and summed to obtain the total induced drag. Several test cases were

used to verify the calculation, and the theoretical limit of  $C_{Di} = C_L^2/(\pi AR)$  was obtained for elliptically loaded wings.

The low-fidelity fluid modeling amounted to simple lifting line theory, conveniently implemented within OPTMIS using a degenerate panel layout, as shown in **Table 4**. Code robustness issues precluded the use of this implementation for the case of the UAV wing planform and, so, for this case, the low-fidelity model consisted of a coarse panel discretization aerodynamic model, the details of which are also furnished in **Table 4**.

**Table 4. Aerodynamic Panel Layout.**

Wing Design Problem	Fidelity Level	Number of Aerodynamic Panels		Spanwise Panel Layout
		Chordwise	Spanwise	
Unswep tapered	High	10	15	Cosine distribution
	Low	1	2	Uniform
UAV, swept	High	10	15	Uniform
	Low	4	7	Uniform

The isotropic material used for the structure was aluminum. We used the following material constants:

**Table 5. Material Properties.**

Material Property	Value
Young's modulus	$10.5 \times 10^6$ lbf/in <sup>2</sup>
Poisson's ratio	0.3
Density	0.1 lb/in <sup>3</sup>
Maximum allowed von Mises stress	$22.5 \times 10^3$ lbf/in <sup>2</sup>

The structural cross section geometry was self-similar as a function of span, and idealized as shown in **Figure 2**. All parameters in **Figure 2** were modeled as being linearly varying from root to tip, with maximum and minimum values indicated in **Table 6**.

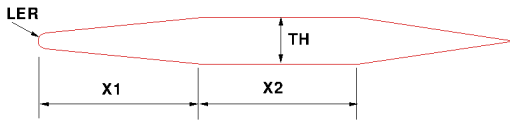


**Figure 2. Structural cross-section.**

**Table 6. Geometric Parameters (ft).**

Geometric Parameters	Tapered wing	UAV wing
X1_root	0.2	0.348
X2_root	0.3	0
TH_root	<i>variable</i>	0.025
X1_tip	0.2	0.103
X2_tip	0.3	0
TH_tip	0.028	0.025
Leading Edge Radius (LER)	0	0

## VII. Results

The results presented in this paper are organized as follows. Convergence results are first presented, followed by computational results. The computational results include comparisons between methods based on single fidelity level results (Section B.1), application of multifidelity optimization to model problems (Section B.2), and multifidelity multidisciplinary design problems involving aeroelastic wings.

### A. Convergence

This section describes rigorous convergence of the methods that we call “hybrid” methods (see earlier section). The convergence proof is obvious and builds on the multifidelity convergence results from Rodriguez, Renaud, and Watson (Ref. 32). Those authors described rigorous results and showed that their trust region method converged under the assumptions they defined. Their results hold for deterministic optimization only and are typical perhaps of nonlinear programming convergence to local minima results. In general, with only a few conditions any downhill search converges. The contribution here relates to the multifidelity aspect of the modeling.

After clarifying their conditions and the trivial convergence of hybrid methods we discuss how some of the conditions used in Ref. 32 might be relaxed and computationally efficient methods might be developed with rigorous guarantees. The hybrid methods are assumed to be likely to offer global results similar to other methods based on global methods and convergence similar to trust region methods. Yet, it is believed further method development will

be needed to achieve both global and rigorous convergence results and the computational efficiency of nonhybrid methods.

### 1. Convergence Conditions

Trust region augmented Lagrangian multifidelity methods have been proven to converge to local optima of the highest fidelity system (Ref. 32). Yet, their assumptions include that the systems are deterministic and that the fidelity level,  $\psi$ , can be continuously adjusted. In the context of multiple local minima they can be considered inferior since sequential optimization methods using global metamodels have been demonstrated on test problems to converge efficiently to the global optimum.

The purpose of this section is to clarify the conditions used to prove the trust region convergence. As a result, reviewing the assumptions from Ref. 32 clarifies the convergence criteria for hybrid methods. It also illuminates the conditions and issues for future, more efficient hybrid optimization method convergence. The list of underlying assumptions can be found Ref. 33.

### 2. Convergence Results

Clearly, if a method can be applied starting at any point and converge, convergence is guaranteed starting from the output of a SRBO or MFSRBO method. Therefore, simple hybrid methods converge if the method used in the last phase converges.

Nontrivial combinations of sequential radial basis optimization (SRBO) and trust region components can certainly be developed that offer computational efficiency advantages and proven convergence benefits. The key issues are the issues for virtually all nonlinear programming methods: (1) maintaining of positive probability of improvement and (2) converging only when the conditions for a local minimum (KKT) are met. Also, the proofs in Ref. 32 are presented in terms of a series of paired levels of fidelity. It seems likely that the key steps can be revised so that the fidelity levels can be discrete and the proof still applies.

## B. Computational Results

The MFSRBO algorithm outlined above was developed, tested, and refined based on a numerical test bed consisting of eight different optimization problems. The main characteristics of these eight problems are outlined in **Table 7**.

**Table 7. Overview of numerical test cases.**

Test Problem Name	Goal / Comment	Multi-		Design Variables	Number of Constraints		
		Disciplinary	Fidelity		Aero.	Structural	
Six hump Branin function	Unconstrained minimization, exhaustive grid-based search, comparison to other methods	no	no	$x_1, x_2$	n/a		
Rosenbrock function & approximation	Unconstrained multifidelity minimization	no	✓	$x_1, x_2$	n/a		
Symmetrized Rosenbrock function & approximation	Multifidelity optimization with two distinct optima	no	✓	$x_1, x_2$	n/a		
Aeroelastic Wing Design	Minimize induced drag, subject to lift and stress constraints	✓	✓	$\alpha_0$	1	1	
“				2	$\alpha_0, d\alpha/ds$	1	1
“				3	$\alpha_0, d\alpha/ds, \theta_0$	1	1
“				4	$\alpha_0, d\alpha/ds, \theta_0, \Lambda$	1	1
UAV Aeroelastic Wing Design	Optimize stability, subject to trim, payload, and stress constraints	✓	✓	$\alpha_0, d\alpha/ds$	2	1	

With the exception of the first test problem (Section B.1), the surrogate search used in each of the optimizations amounts to a multistart steepest ascent scatter-and-poll strategy (Ref. 24) for calculating  $\arg(\max(EI(\mathbf{x}, l)))$ .

### 1. Single Fidelity Level Results

The single fidelity results presented in this section are almost the same as in Refs. 16 and 26. This follows because in virtually all of the test problems good solutions were obtained from the initial design portions which were identical between the Kriging model and radial basis function-based approaches. In all of the problems in Ref. 16, for example, fewer than 25% of the evaluations were after the initial design evaluations. First, we consider the single fidelity noisy case for simplicity.

In the results shown below the Sequential Radial Basis Optimization (SRBO) method is empirically compared with three alternative approaches from the literature. The first alternative is the Simultaneous Perturbation Stochastic Approximation (SPSA) from Spall (Ref. 34). The second approach is the Revised Simplex Search (RSS) procedure, a variant of the Nelder-Mead method, proposed by Humphrey and Wilson (Ref. 35). As the original RSS procedure was not designed to handle constraints, we modify it so that whenever a point is infeasible, the algorithm selects the nearest feasible point instead. The third approach is the DIRECT method developed by Gablonsky (Ref. 36) et al.

Here, we focus on a single fidelity system with noise. In this case, the test function is the six hump camelback function from Branin (Ref. 37) with  $\sim N(0, 0.122)$  noise added. The function is:

$$f(\mathbf{x}) = 4x_1^2 - 2.1x_1^4 + x_1^6/3 + x_1x_2 - 4x_2^2 + 4x_2^4$$

$$-1.6 \leq x_1 \leq 2.4, \quad -0.8 \leq x_2 \leq 1.2$$

$$\mathbf{x}^* = (0.089, -0.713) \wedge (-0.089, 0.713), \quad f^* = -1.03$$
(24)

In this problem, there are six local and two global optima. For the single fidelity, noisy case, the expected improvement function (Eq. (17)) simplifies with  $\alpha_1 = \alpha_3 = 1$ .

**Figure 3** plots two randomly selected sequential radial basis optimization (SRBO) runs overlaid on the results of four alternative methods. The SRBO method was applied using  $\gamma = 0.5$  and  $r = 3$ , i.e., the last three runs are used for the residual. The results indicate that SRBO methods converge quickly like sequential Kriging optimization (SKO) methods. Possible convergence issues are believed to relate to the  $100 \times 100$  grid used for expected improvement optimization. It is also possible that the convergence is limited by the constant  $\gamma$ , which explains why variations of  $\gamma$  were conducted in our aerospace wing case study (Section B.3).

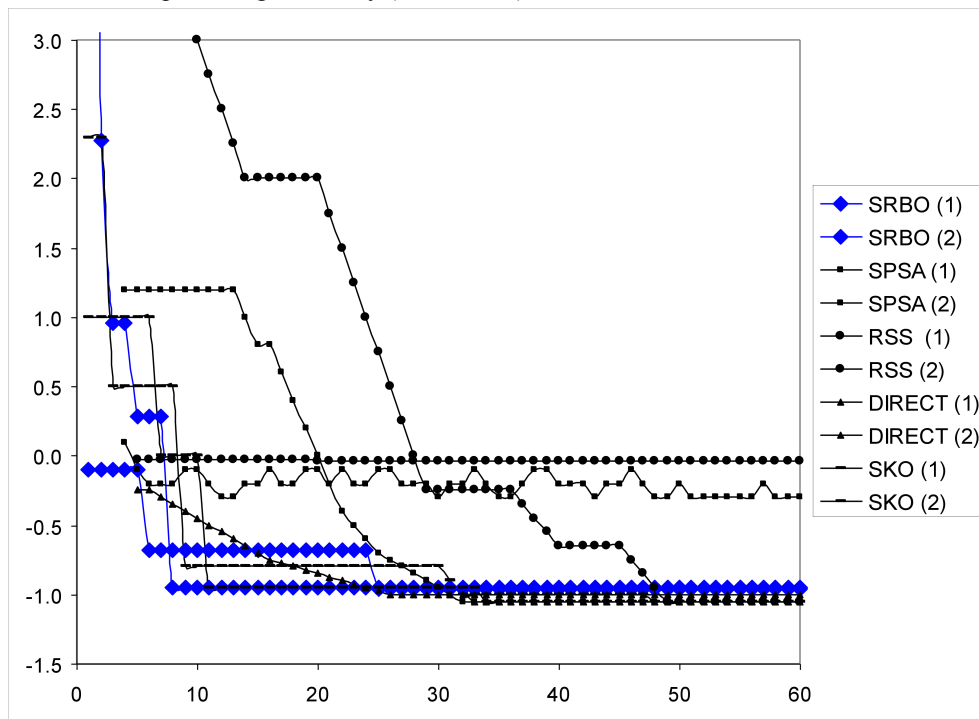


**Figure 3.** Results from two randomly selected runs of each method on the six hump camel back function. (Vertical axis corresponds to the function value. Horizontal axis corresponds to the number of function calls).

## 2. Multifidelity Test Problem

The application of the augmented dimensionality variant of multifidelity sequential radial basis optimization (MFSRBO) to Rosenbrock's function is considered next. Similarly to Eldred et al. (Ref. 38), we consider the minimization of Rosenbrock's function (**Figure 4**):

$$f_{HF} = 100(x_2 - x_1^2)^2 + (1 - x_1)^2 \quad (25)$$

$f_{HF}$  is the true (high-fidelity) function to be minimized. Its low-fidelity surrogate  $f_{LF}$  is defined as

$$f_{LF} = 100(x_2 - x_1^2 + 0.2)^2 + (0.8 - x_1)^2 \quad (26)$$

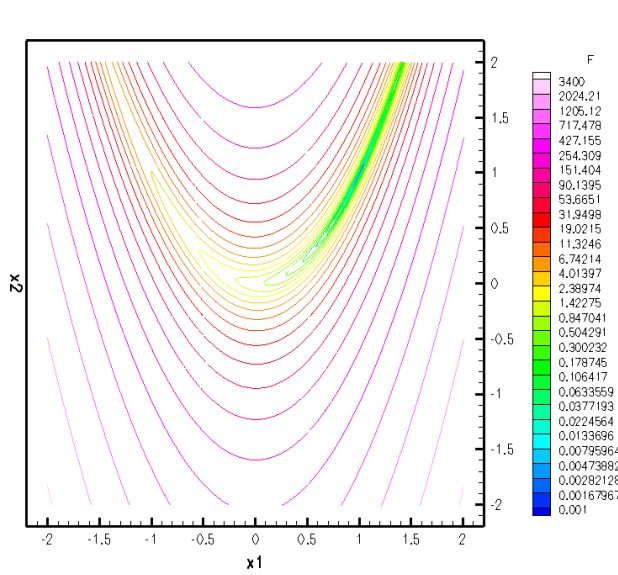


**Figure 4. Isocontours of the high-fidelity Rosenbrock function.**

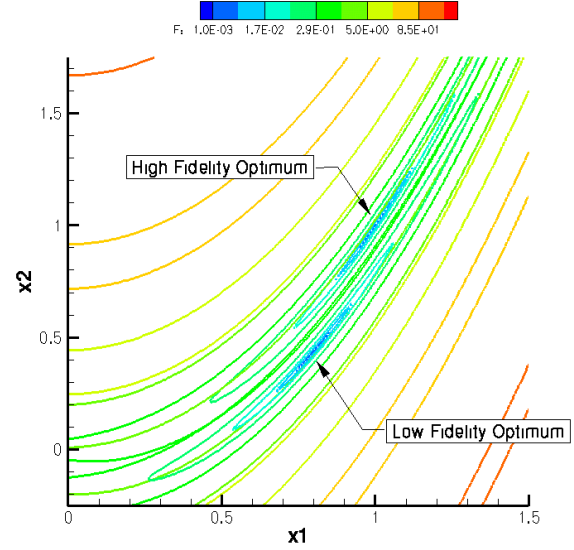


**Figure 5. Comparison between the Rosenbrock function and its low-fidelity counterpart in the vicinity of their optima.**

Whereas the two functions have similar structure, the high-fidelity function has its minimum at  $(x_1 = 1, x_2 = 1)$ , the low-fidelity one at  $(x_1 = 0.8, x_2 = 0.44)$ . The two functions are not, in the strictest sense, weakly consistent, but the problem has favorable structure. In the immediate vicinity of the high-fidelity optimum  $f_{HF} = 0$  but  $f_{LF} \approx 4$  and the *difference* between the two models exhibits strong gradients, as illustrated in **Figure 5**.

Because the methods described in Section IV integrate data at all levels of fidelity to build a global radial basis function metamodel, it is possible to use the associated Multifidelity Expected Improvement function (Eq. (17)) as the criterion determining the location and fidelity level of subsequent evaluations:

$$EI(\mathbf{x}, k) \stackrel{\text{def}}{=} E \left[ \max(\hat{f}_m(\mathbf{x}^*) - \hat{f}_m(\mathbf{x}) - \sigma_m(\mathbf{x})\epsilon, 0) \right] \cdot \text{corr}[\hat{f}_k(\mathbf{x}), \hat{f}_m(\mathbf{x})] \cdot \left( 1 - \frac{\hat{\sigma}_{0,k}}{\sqrt{\hat{\sigma}_k^2(\mathbf{x}) + \hat{\sigma}_{0,k}^2}} \right) \cdot \frac{\text{Cost}_m}{\text{Cost}_k} \quad (27)$$

where  $\hat{f}_m(\mathbf{x})$  is the high-fidelity prediction at point  $\mathbf{x}$ , and  $\mathbf{x}^*$  is the current “effective best solution” defined in Eq. (20).  $\hat{\sigma}_{0,k}^2$  is the unexplained variance of the radial basis function model at level  $k$ , and  $\hat{\sigma}_k^2(\mathbf{x})$  is the variance of  $\hat{f}_k(\mathbf{x})$ . The correlation term  $\text{corr}[\hat{f}_k(\mathbf{x}), \hat{f}_m(\mathbf{x})]$  is used to discount the expected improvement when an evaluation from a lower fidelity surrogate is used. The term involving  $\hat{\sigma}_{0,k}^2$  accounts for diminishing returns of additional replicates as the prediction becomes more accurate, and the cost ratio adjusts the sampling strategy according to the evaluation costs (Ref. 16). The location and fidelity of the next evaluation,  $\mathbf{x}_{n+1}$  and  $k_{n+1}$  are given by maximizing  $EI(\mathbf{x}, k)$ , i.e.:

$$(\mathbf{x}_{n+1}, k_{n+1}) = \arg(\max(EI(\mathbf{x}, l))) \quad (28)$$

The effective best solution  $\mathbf{x}^*$  is defined by  $\mathbf{x}^* = \arg(\max(u(\mathbf{x})))$  where  $u(\mathbf{x}) = -\hat{f}_m(\mathbf{x}) - \mu \sigma_m(\mathbf{x})$  expresses the willingness to trade one unit of the predicted objective for  $\mu$  units of the standard deviation of the prediction uncertainty (Ref. 23). Also, the expectation in  $EI(\mathbf{x}, k)$  is conditional given the past data and given estimates of the correlation parameters. Thus, the expectation is computed by integrating over the distribution of  $\hat{f}_m(\mathbf{x})$ , with  $\hat{f}_m(\mathbf{x}^*)$  fixed. Specifically, assuming a normally distributed error, the *probability of improvement*  $P[\hat{f}_m(\mathbf{x}) < \hat{f}_m(\mathbf{x}^*)]$  is given by

$$P[\hat{f}_m(\mathbf{x}) < \hat{f}_m(\mathbf{x}^*)] = \frac{1}{s_m(\mathbf{x})} \int_{-\infty}^{\hat{f}_m(\mathbf{x}^*)} \varphi(y - \hat{f}_m(\mathbf{x}); s_m(\mathbf{x})) dy \quad (29)$$

where  $\varphi$  is the probability density function:

$$\varphi(y; \sigma) = \frac{1}{\sqrt{(2\pi)}} \exp\left(-\frac{y^2}{2\sigma^2}\right) \quad (30)$$

As pointed out in Ref. 9, the *expected improvement* is the first moment of Eq. (29), i.e.,

$$EI|_{\hat{f}_m(\mathbf{x}) < \hat{f}_m(\mathbf{x}^*)} = \frac{1}{s_m(\mathbf{x})} \int_{-\infty}^{\hat{f}_m(\mathbf{x}^*)} (\hat{f}_m(\mathbf{x}) - y) \cdot \varphi(y - \hat{f}_m(\mathbf{x}); s_m(\mathbf{x})) dy \quad (31)$$

After integration by parts, the expectation can be calculated analytically as follows:

$$E\left[\max(\hat{f}_m(\mathbf{x}^*) - \hat{f}_m(\mathbf{x}), 0)\right] = (\hat{f}_m(\mathbf{x}^*) - \hat{f}_m(\mathbf{x})) \cdot \Psi(\hat{f}_m(\mathbf{x}^*) - \hat{f}_m(\mathbf{x}); s_m(\mathbf{x})) + s_m(\mathbf{x}) \cdot \varphi(\hat{f}_m(\mathbf{x}^*) - \hat{f}_m(\mathbf{x}); s_m(\mathbf{x})) \quad (32)$$

where  $\varphi$  is the normal probability density function defined above, and  $\Psi$  is the normal cumulative distribution function:

$$\Psi(y; \sigma) = \frac{1}{2} \left[ 1 + \operatorname{erf}\left(\frac{y}{\sqrt{2}\sigma}\right) \right] \quad (33)$$

For the multifidelity Rosenbrock function, the initial design consisted of four points (the four corners in **Figure 4**), three of which were chosen to be low-fidelity. The fourth, high-fidelity corner was chosen randomly. An assumed data point uncertainty ( $\sigma_0$  in Eq. (14)) of 0.01 was used.<sup>4</sup> A typical optimization result is shown in **Figure 6** which depicts the search path history. In **Figure 6** the low-fidelity function evaluations are identified by the small symbols and the high-fidelity ones with the larger symbols.

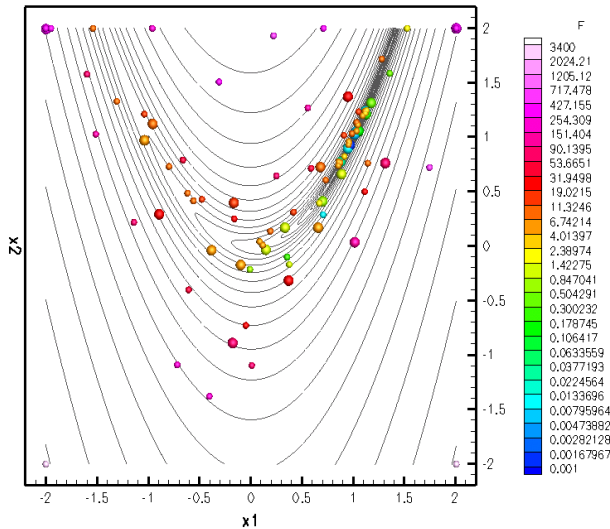


**Figure 6. Multifidelity search path and isocontours of the high-fidelity Rosenbrock function.**

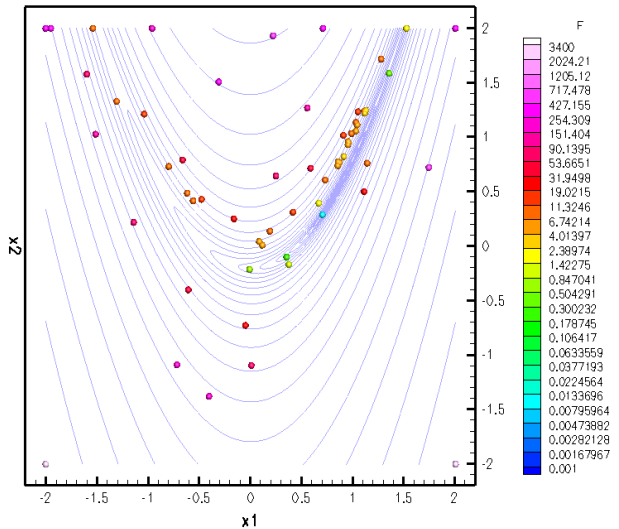


**Figure 7. Low-fidelity subset of multifidelity search path with isocontours of the low-fidelity Rosenbrock function.**

The optimization correctly identifies the high-fidelity optimum in a relatively small number of high-fidelity function evaluations. For reference, **Figure 7** shows the low-fidelity subset of **Figure 6**, super-imposed on isocontours of the low-fidelity function. This picture helps understand the role of the low-fidelity evaluation as an aid to sample the design landscape. Note in particular the accumulation of points near the high-fidelity optimum ( $x_1 = 1, x_2 = 1$ ), and not the low-fidelity one ( $x_1 = 0.8, x_2 = 0.44$ ).

<sup>4</sup> for purposes of comparison with the Branin function example considered in the previous section, this data point uncertainty can be thought of as  $\sim N(0, 0.01)$  “virtual” noise

In the results depicted in **Figures 6** and **7** the assumed cost ratio between the two fidelity levels was  $3/2$ . As expected, the multifidelity expected improvement function drives the objective towards the high-fidelity optimum and takes advantage of the presumed-low-cost, low-fidelity evaluations to find a positive direction of improvement. The approach is successful because the cumulative radial basis function metamodel is able to “learn” the relationship between the low- and high-fidelity projections. In an ideal sense, this nonlinear relationship must be accurately defined using as few (expensive) high-fidelity observations as possible. Our empirical observations suggest that, because the uncertainty on this relationship remains large if the high-fidelity observations are too few, there is a practical tradeoff which must be considered in the initial design. For the majority of our experiments, the ratio of high-fidelity to low-fidelity initial count was around 25%.

To further demonstrate the method on a problem exhibiting more than one local optimum, we considered the following dual optimum problem, constructed by smooth-symmetrizing the Rosenbrock function about the origin as follows:

$$h(x_1, x_2) = \eta \cdot f(x_1, x_2) + (1 - \eta) \cdot f(-x_1, -x_2)$$

$$\eta = \frac{1}{2} (\tanh[20(x_1 + x_2)] + 1)$$
(34)

In Eq. (34)  $f$  designates either  $f_{HF}$  or  $f_{LF}$  as appropriate. As in the previous example, the initial design consists of the four corner points ( $x_1 = \pm 2, x_2 = \pm 2$ ), only one of which is evaluated at the high-fidelity level.

**Figure 8** shows the multifidelity search path obtained by MFSRBO with an assumed  $3/2$  cost ratio and an assumed  $\sigma_0 = 0.01$ . As in **Figure 6**, the small symbols in the figure represent the results of low-fidelity analyses, and the large symbols correspond to high-fidelity analyses. It is noteworthy that, regardless of the fidelity at which they are calculated, the accumulated designs find both optima of the *high-fidelity* function,  $h_{HF}$ .

The convergence history is illustrated in **Figure 9**, which shows on a semi-log scale the values  $h_{HF}(x_1, x_2)$  of the high-fidelity infills, in their order of appearance. In order for the optimization to be able to both *explore* the design landscape and *exploit* the narrow minima, it is advantageous to relax the metamodel stiffness (i.e., increase  $\gamma$  or  $\gamma_i$ ) as the design progresses. In its present implementation, this adaptivity is based on a simple, heuristic algorithm. This algorithm increases the  $\gamma_i$  parameters by a small factor

$$\gamma_i^{NEW} = (1 + \tau_1) \gamma_i^{OLD}$$
(35)

anytime the rank of the linear model design matrix  $\mathbf{X}$  recedes below a given percentage of its full rank:

$$\frac{\text{rank}(\mathbf{X})}{n} \leq \tau_2$$
(36)

For example, the results of **Figures 8** and **9** were obtained using  $\tau_1 = 0.11$  and  $\tau_2 = 0.94$ .

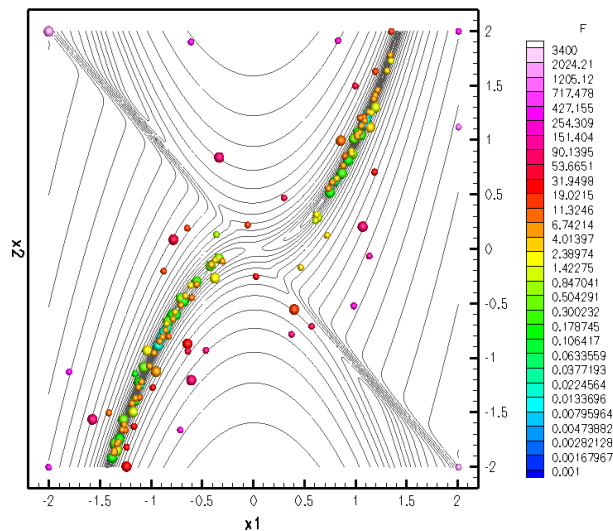


**Figure 8.** Multifidelity search path superimposed with isocontours of the high-fidelity symmetrized Rosenbrock function.

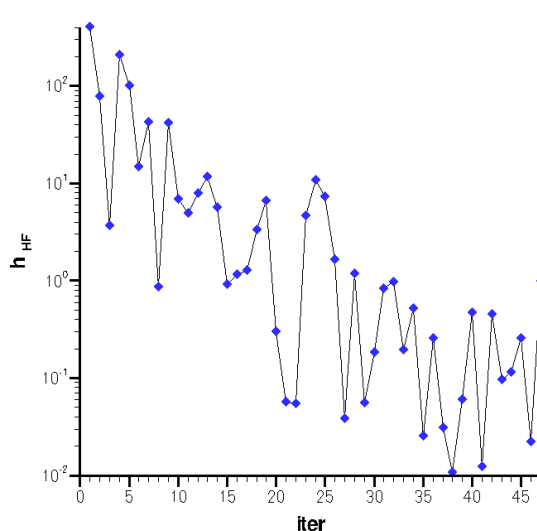


**Figure 9.** History of high-fidelity infills corresponding to the multifidelity optimization search path shown in **Figure 8**.

### 3. Aeroelastic Wing Design Problem

Two aeroelastic wing design problems were considered as part of this investigation. The first, designated “baseline problem,” consisted of an aspect ratio 10 unswept rectangular or slightly tapered wing designed for minimal drag under load. The second problem, referred to as the “UAV wing design,” was aimed at maximizing longitudinal aerodynamic stability, and was characterized by the incorporation of multiple constraints and a noisy objective function.

#### 3.1 Baseline Problem

A baseline problem was defined for the purpose of developing and demonstrating the MFSRBO approach and its ability to represent and integrate information from each discipline and model. Computational fluid dynamics (CFD) and computational structural mechanics (CSM) were initially targeted as examples of high-fidelity models for the two interacting disciplines (fluids and structures). However, the practical realities of time frame and budget focused our attention instead on the following analysis methods and fidelity levels (see Section VI):

**Table 8. Overview of computational methods used.**

MODELS	Fluids	Structures
<b>High Fidelity</b>	OPTMIS/MISDL, intermediate-level aerodynamic prediction code based on panel methods and other classical singularity methods enhanced with models for nonlinear vortical effects. Applicable to subsonic and supersonic flight vehicles including aircraft, UAVs, missiles, and rockets.	CNEVAL FEM method; provides weights, displacements, stresses, and modal frequencies.
<b>Low Fidelity</b>	Lifting line theory, supplemented with induced drag calculation.	Low degree-of-freedom version of the CNEVAL FEM model.

An analysis of baseline problem candidates led to the selection of the minimum drag design of a wing subject to minimum lift and static aeroelastic constraints as the focus of this demonstration. This benchmark problem is derived from Robinson et al. (Refs. 4, 5). It seeks to minimize the induced drag  $C_{D,i}$  by changing the pre-load twist distribution (parameterized here by the root chord angle of attack  $\alpha_0$  and its spanwise first and second derivatives,  $d\alpha/dy$  and  $d^2\alpha/dy^2$ ). Two additional variables are introduced: the root chord maximum structural thickness  $\theta_0 \stackrel{\text{def}}{=} \text{TH}(y=0)$ , and the taper ratio  $\Lambda \stackrel{\text{def}}{=} c_{tip}/c_{root}$  of the unswept flexible wing. The wing span is maintained constant,  $y_{max} = 5 \text{ ft}$ , and the wing area is also kept fixed, at  $S = 5 \text{ ft}^2$ .

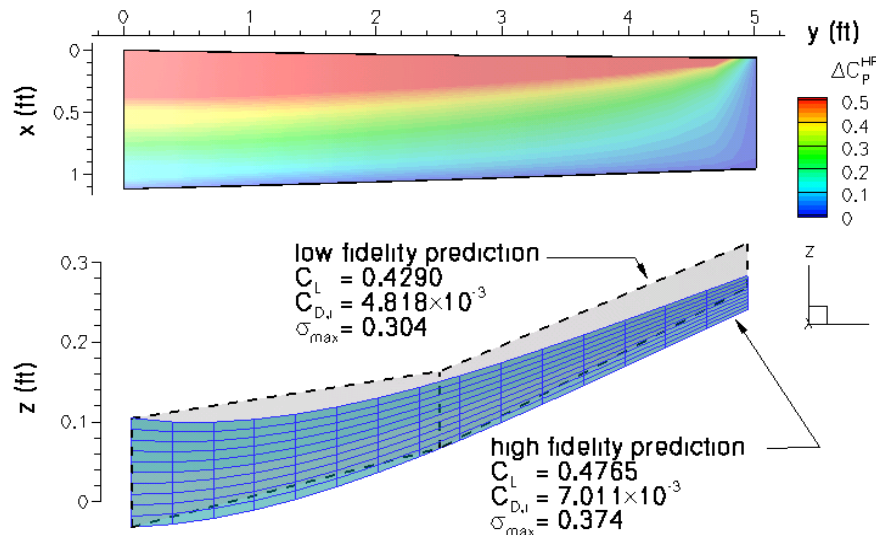


**Figure 10. Low- and high-fidelity static aeroelastic deformation prediction. (Top: aerodynamic loading (planform view). Bottom: streamwise view of combined wing twist and bending (not to scale)).**

The induced drag was minimized, subject to minimum lift and maximum stress constraints as follows:

$$\begin{aligned} & \text{minimize} && C_{D,i} \\ & \{ \alpha_0, d\alpha/ds, \theta_0, \Lambda \} \\ & \text{subject to} && C_L \geq (W_{\text{payload}} + W_{\text{wing}})/(q_\infty S_{\text{ref}}) \\ & && \sigma_{VM} / \sigma_{VM,max} < 0.5 \end{aligned} \quad (37)$$

where  $\sigma_{VM}$  is the von Mises stress,  $W$  is weight,  $q_\infty$  is dynamic pressure, and  $S_{ref}$  is the wing reference area. For this investigation, the freestream angle of attack is zero, the freestream Mach number is  $M_\infty = 0.2$ , the dynamic pressure is  $q_\infty = 40.76 \text{ psf}$ , and the assumed payload is  $W_{\text{payload}} = 75 \text{ lbs}$ .

A typical comparison of low- and high-fidelity analyses<sup>5</sup> is given in **Figure 10**,<sup>6</sup> corresponding to  $\alpha_0 = 7^\circ$ ,  $d\alpha/ds = -0.8^\circ \text{ft}^{-1}$ ,  $d^2\alpha/ds^2 = 0^\circ \text{ft}^{-2}$ ,  $\theta_0 = 0.045 \text{ ft}$ , and  $\Lambda = 0.8$  using the material and cross-sectional properties shown in Section VI.

One-, two-, three-, and four-dimensional variations on the minimum drag aeroelastic wing design problem were investigated as part of this effort. To better understand how the optimization method performed on these cases, let us consider the two-dimensional results (**Table 7**, subcase 2) in which a fixed root chord maximum thickness  $\theta_0 = 0.04 \text{ ft}$  and fixed taper ratio  $\Lambda = 1$  are used.

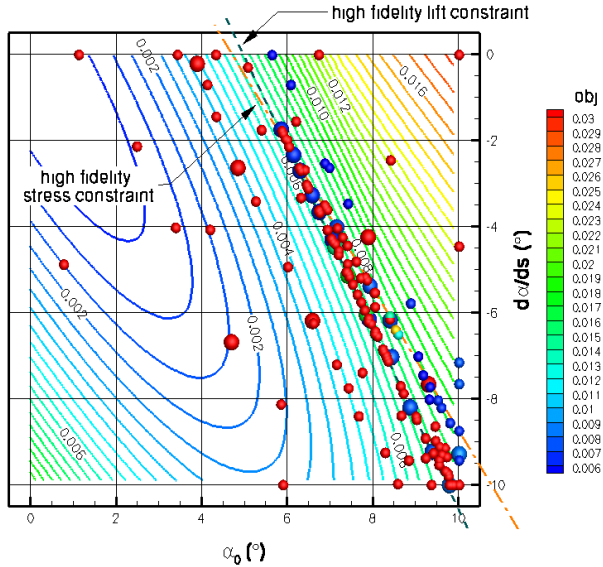


**Figure 11. Sample multifidelity search path for two-dimensional aeroelastic wing design problem.**

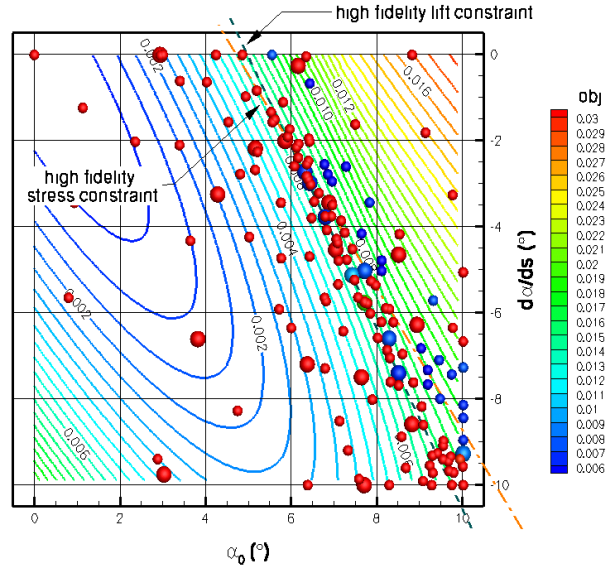


**Figure 12. A different instantiation of the problem solved in Figure 11 (different initial conditions).**

**Figures 11 and 12** provide two examples of the MFSRBO search path when the optimization is initiated from two randomly chosen Latin Hypercube design of experiments, each including one high-fidelity and three low-fidelity solutions (see **Table 9**).

**Table 9. Listing of initial conditions**

Point Number	Initial Design Used in Figure 11			Initial Design Used in Figure 12		
	$\alpha_0$ ( $^\circ$ )	$d\alpha/ds$ ( $^\circ$ )	Fidelity level	$\alpha_0$ ( $^\circ$ )	$d\alpha/ds$ ( $^\circ$ )	Fidelity level
<b>1</b>	8.405	-2.453	Low	<b>3.021</b>	<b>-9.752</b>	<b>High</b>
<b>2</b>	0.784	-4.876	Low	7.487	-1.617	Low
<b>3</b>	<b>4.690</b>	<b>-6.679</b>	<b>High</b>	9.019	-6.821	Low
<b>4</b>	5.851	-8.127	Low	0.934	-3.438	Low

<sup>5</sup> The cost ratio between high- and low-fidelity analyses was 5:1

<sup>6</sup> “ $\sigma$ ” in Figure 10 denotes the ratio  $\sigma_{VM} / \sigma_{VM,max}$

The following computational analysis uncertainties ( $\sigma_0$  in Eq. (14)) were used uniformly for the OPTMIS outputs:

**Table 10. OPTMIS output uncertainties**

	$C_L$	$C_{D,i}$	$W_{wing}$ (lb)	$\sigma_{VM}/\sigma_{VM,max}$
$\sigma_0$	0.0002	0.002	0.03	0.02

The results of **Figures 11 and 12** are shown as a function of the two design variables  $\alpha_0$  and  $d\alpha/ds$ , where  $s$  is the nondimensional span variable,  $s = y/y_{max}$ . The background contour lines represent the high-fidelity primary (unconstrained) objective,  $C_{D,i}$ . The large symbols denote high-fidelity analyses, whereas the small symbols represent the low-fidelity analyses. Each symbol is colored based on the objective function, which is the induced drag  $C_{D,i}$ , modified with penalty functions for violating lift and/or stress constraints (themselves indicated by dashed lines). Specifically, the constraints are incorporated into the objective function using the following penalty formulation (using the previously quoted values for  $W_{payload}$ ,  $q_\infty$  and  $S_{ref}$ ):

$$f = C_{D,i} + 10 \cdot \max \left[ \left( \frac{75 + W_{wing}}{40.76 \times 5} \right) - C_L, 0 \right] + 20 \cdot \max \left[ \frac{\sigma_{VM}}{\sigma_{VM,max}} - 0.5, 0 \right] \quad (38)$$

where  $W_{wing}$  is the structural weight of the wing, expressed in pounds. The process of maximizing the multifidelity expected improvement function (17) involves calculating (21), which requires keeping track of the current best effective solution  $x^* = [\alpha_0^*, (d\alpha/dy)^*, \theta_0^*, \Lambda^*]$ , and the ability to estimate the objective function  $f$  and its variance  $s^2$  at any design point  $x$  for any level of fidelity.

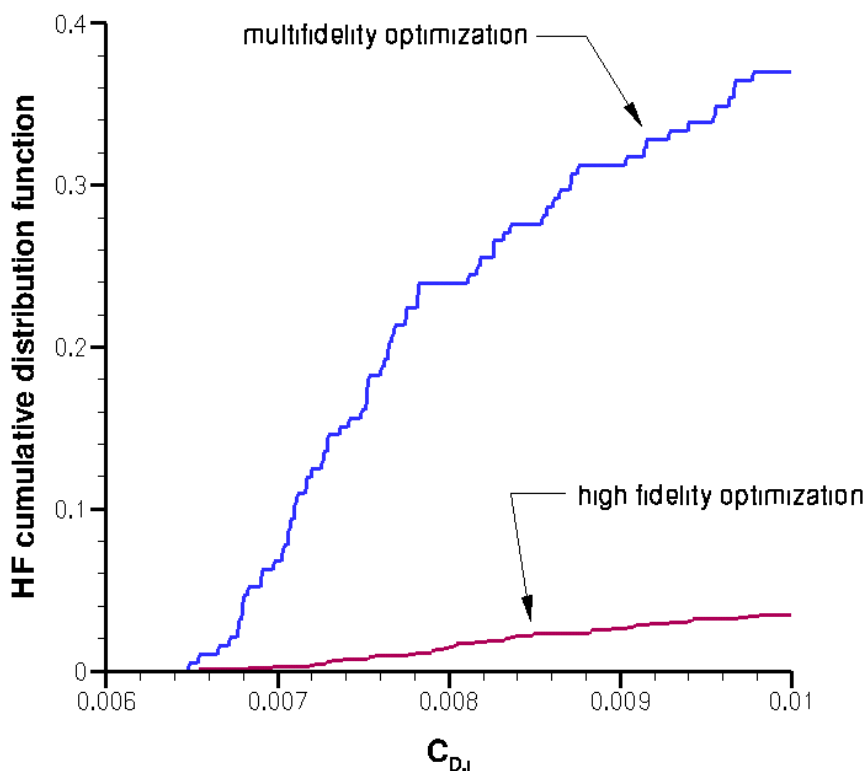


**Figure 13. Quantification of multifidelity vs. high-fidelity-only optimization performance via aggregated cumulative distribution functions. The primary objective,  $C_{D,i}$  is shown on the horizontal axis. The vertical axis is the numerically computed probability of finding feasible high-fidelity solutions meeting the target on the x axis.**

A more elegant way of handling the constraints in a consistent and fully probabilistic manner is described in Forrester et al. (Ref. 9). The detailed implementation of this method applied to the present problem is described in Ref. 33.

### Statistical Results

It is important to realize that, due to the inherent coupling between the optimization path and the sequential radial basis function metamodel being created at the various stages of the optimization, the results depend on the initial conditions of the optimization (this is true whether one uses multifidelity or single fidelity optimization). **Figure 12**, for example, presents a different data profile for the same nominal problem as **Figure 11**, the only difference being the initial conditions.

For this reason, when comparing performance metrics, it is particularly important to collect multiple results such as **Figures 11 and 12** and to consider ensembles in a statistical sense in order to draw meaningful conclusions. Thus, using multiple realizations with random initial conditions based on a Latin Hypercube design of experiments, optimization results were aggregated and analyzed as a group. When comparing multifidelity vs. high-fidelity-only optimization, care must also be exercised so that the exact same design variables are used in the initial design.

The details of this aggregate analysis are as follows. The candidate designs harvested as a result of each optimization are first filtered so that only the high-fidelity (HF) solutions that do not violate the constraints are considered.<sup>7</sup> These HF nonviolators are then sorted based on the primary objective (low  $C_{D,i}$  in the present case). Aggregate performance profiles collected in this manner can then be analyzed in terms of the induced drag cumulative distribution function (CDF) of the wing designs. The example shown in **Figure 13** corresponds to 8 realizations of the three-dimensional optimization (**Table 7** subcase 3). The stopping criterion was based either on failure to improve the EI function (Eq. (17)), or reaching a self-imposed computational budget consisting of a maximum of 24 high-fidelity evaluations. The optimal designs for this case (i.e., **Table 7** subcase 3) are given in the table below:

Method	$\alpha_0$ (°)	$d\alpha/dy$ (°ft <sup>-1</sup> )	$\theta_0$ (ft)	$C_L$	$C_{D,i}$	$W_{wing}$ (lbs)	$\sigma_{VM}$
MFSRBO	6.624	-0.704	0.0392	0.4624	$6.484 \times 10^{-3}$	18.87	0.442
HF-only	6.418	-0.603	0.0384	0.4643	$6.542 \times 10^{-3}$	18.64	0.471

**Figure 13** shows that, by using multifidelity optimization, there is, for example, a 37% probability of achieving a drag coefficient less than 0.01, versus less than 4% with high-fidelity optimization only. Thus, for a given computational budget, there is an order of magnitude greater probability of finding/approaching the high-fidelity optimum by using multifidelity optimization.

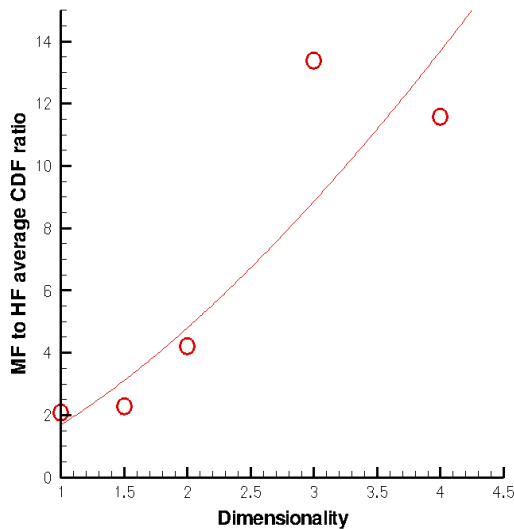


**Figure 14. Relative efficiency between multifidelity (MF) and high-fidelity (HF)-only optimization as a function of design space dimensionality.**

in scope and strictly empirical, the results of **Figure 14** suggest the possibility that the MFSRBO method may be increasingly beneficial as the dimensionality of the problem increases, although this question will be left for future research.

Neglecting, for the sake of simplicity, the cost of the low-fidelity analyses and the cost of the optimization calculations *per se*, the average ratio of the cumulative distribution functions provides an indication of the relative performance of these methods. Let us define the CDF area ratio as the ratio between the areas under the CDF curves (**Figure 13**) for  $C_{D,i} \leq 0.01$ .

**Figure 14** shows the CDF area ratio as a function of the search space dimensionality of the problem. The three- and four-dimensional cases are believed to be more typical of the expected performance ratio. Our observations suggest that the replicate-deterrent term ( $\alpha_2$  in Eq. (19)), may have had an important effect in the lower dimensional experiments, due to the effectively higher point density in those cases. The one-dimensional case was obtained by varying  $\alpha_0$  only. (The so-called “1.5-dimensional” case represents a case where the constraints were such that only a narrow sliver of feasible solutions existed in the nominally 2-D space, thus making the space effectively quasi-one-dimensional). Although limited

<sup>7</sup> In this study, this was typically repeated for 8 to 16 realizations.

### 3.2 UAV Wing Design

The baseline problem described above was extended to the case of an aeroelastic swept (UAV-type) wing at  $M_\infty = 0.2$ . The wing planform is a modified version of the European *SACCON* stability and control vehicle<sup>8</sup> with identical span and wing area. As in **Table 7** subcase 2 above, the design variables are the pre-load twist distribution parameters,  $\alpha_0$  and  $d\alpha/ds$ . However, this time, the design objective is to maximize longitudinal pitch stability,  $-dC_m/d\alpha$ , subject to minimum lift, maximum stress, and trim/controllability constraints, as follows:

$$\begin{aligned} & \text{minimize} && dC_m/d\alpha \\ & \{\alpha_0, d\alpha/dy\} \\ & \text{subject to} && C_L \geq (W_{\text{payload}} + W_{\text{wing}})/(q_\infty S_{\text{ref}}) \\ & && \sigma_{VM} / \sigma_{VM, \max} < 0.55 \\ & && |C_m| < 0.002 \end{aligned} \quad (39)$$

where  $C_m$  is the pitching moment about the root half chord location.

An example comparison of low- and high-fidelity results obtained using OPTMIS is shown in **Figure 15**,<sup>9</sup> corresponding to  $\alpha_0 = 18.5^\circ$ ,  $d\alpha/dy = -4.3^\circ \text{ft}^{-1}$  and  $W_{\text{payload}} = 75 \text{ lbs}$  for an isotropic material with self-similar cross-section (see Section VI) and a spanwise-uniform maximum thickness of  $\theta_0 = 0.025 \text{ ft}$ .

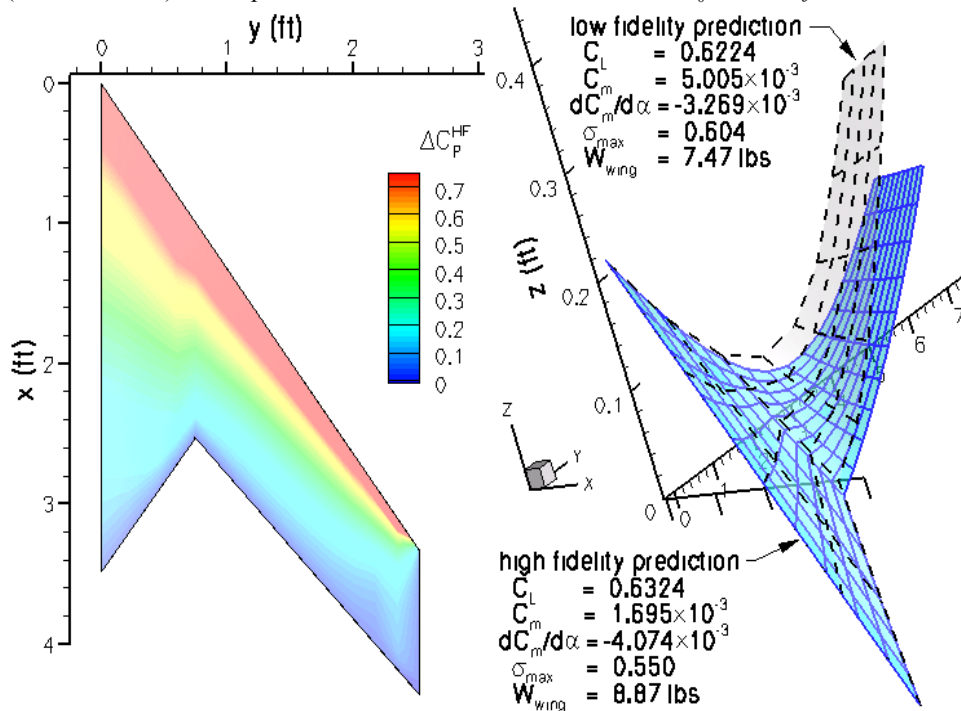


**Figure 15. Low- and high-fidelity static aeroelastic deformation of UAV wing. (Left: planform view of loading. Right: perspective view of wing twist and bending (not to scale)).**

The optimization methods and postprocessing metrics were identical to those described in Section 3.1. **Figure 16** provides an illustration of the multifidelity sequential radial basis optimization search path for a given instance of a Latin Hypercube design of experiments including one high-fidelity and three low-fidelity solutions as the initial conditions. The flooded contours represent the primary objective,  $dC_m/d\alpha$ , which is noisy, due in part to finite differencing and to  $C_m$  being itself a sensitive quantity. As before, the large symbols denote high-fidelity analyses, whereas small symbols are used for low fidelity. Each symbol is colored based on the objective function, which is the stability derivative  $dC_m/d\alpha$ , augmented with penalty functions for violating either the lift, trim, or stress constraints. Specifically, the

<sup>8</sup> NATO RTO, AVT-161 Assessment of Stability and Control Prediction Methods for NATO Air & Sea Vehicles.

<sup>9</sup> “ $\sigma$ ” in Figure 15 denotes the ratio  $\sigma_{VM} / \sigma_{VM, \max}$

constraints are incorporated in the objective function using the following penalty formulation (using the previously quoted values for  $W_{\text{payload}}$ ,  $q_{\infty}$ , and  $S_{\text{ref}} = 4.15 \text{ ft}^2$ ):

$$\begin{aligned}
 f = & \frac{dC_m}{d\alpha} + 10 \cdot \max[|C_m| - 0.002, 0] \\
 & + 10 \cdot \max\left[\left(\frac{75 + W_{\text{wing}}}{40.76 \times 4.15}\right) - C_L, 0\right] \\
 & + 20 \cdot \max\left[\frac{\sigma_{VM}}{\sigma_{VM, \max}} - 0.5, 0\right]
 \end{aligned} \tag{40}$$

where  $W_{\text{wing}}$  is the structural weight of the wing, expressed in pounds.

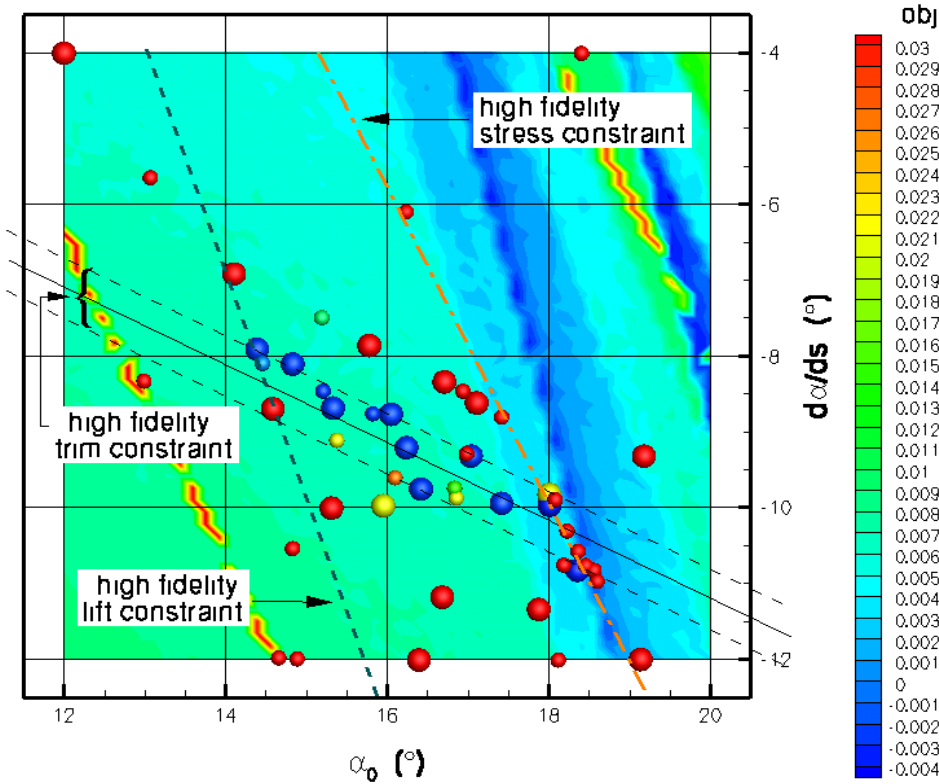


**Figure 16. Sample multifidelity search path for UAV aeroelastic wing design problem.**

Aggregate cumulative distribution functions for the multifidelity and high-fidelity-only optimizations were determined for this problem, in a manner similar to **Figure 13**. The resulting CDF area ratio, defined as the ratio between the areas under the CDF curves for  $dC_m/d\alpha \leq -0.0027$ , suggests 4:1 odds in favor of multifidelity optimization, as indicated in **Figure 14**.

## VIII. Concluding Remarks / Discussion

This paper has explored the use of radial basis functions rather than Kriging models in sequential multifidelity optimization. In adapting the methods, we have addressed at least three types of unavoidable challenges relating prediction, error estimation, and the expected improvement function. This investigation explored proposing two types of metamodeling approaches which are (a) *cascading* (the most direct extension of Kriging-based methods with convergent prediction) and (b) *augmented dimensionality* (which offers advantages for data starved cases).

Perhaps the greatest challenge was developing a comprehensive estimate of uncertainty corresponding to the approximate Bayesian intervals for Kriging functions. They are approximate because they are based on parameter estimates. Here, four types of approaches were considered with numerical results based on assumed errors and simple

cross-validation. Finally, two alternative formulations for the expected improvement function were described because of the computational challenge of estimating correlation for the radial basis function case.

The preliminary numerical results indicate that methods based on radial basis functions can compete with Kriging methods in relation to efficiently and repeatedly identifying global optimal solutions. Based on the numerical testing conducted thus far, the advantages and disadvantages of the proposed radial basis function approach can be summarized as follows:

**Reduced computational overhead** – Radial basis function estimation does not require likelihood minimization since a closed form is used for the coefficient estimates. By contrast, thorough and accurate likelihood optimization is a difficult computational challenge. The efficiency increase realized by eliminating one of the two optimizations per iteration (the other being the expected improvement optimization) can enable many new applications of related methods. These include “on-line” or automatic optimal decision-making. For example, data can stream in from sensors or simulations running in parallel, and can be quickly integrated for determining optimal settings and requests for additional inputs.

**Improved numerical stability** – In contrast to prior computational work (e.g., Huang, Allen, Notz, and Miller (Ref. 16)), radial basis function fitting is based on linear model estimation which is very stable.

**Error estimation including bias** – The errors used in the proposed MFSRBO are based on regression variance errors only. This makes their interpretation difficult in deterministic cases, i.e., cases with perfect repeatability error or  $\sigma = 0$ . In such cases, the intervals do not directly correspond to any interpretable physical quantity in the corresponding problem and performance of the methods likely is degraded. Developing new methods based on measures of bias such as the diagnostics proposed in Tseng (Ref. 28) may constitute a promising avenue of research.

**Measuring computational overhead** – It is clear that linear model estimation is computationally superior to likelihood estimation in Kriging models. Yet, so far we have not measured the computational advantages. Also, we have not tuned the methods to the point at which the overhead is minimal and comparable to standard nonlinear programming methods. The promising results from the radial basis function methods here suggest that such performance is achievable.

**Parallelizing the methods** – One promising area is the possibility of parallelizing function evaluations. For example, it is advantageous to launch one slow, high-fidelity simulation simultaneous with several low-fidelity simulations. The structure of these methods lends itself nicely to parallel processing with its significant computational advantages.

## Acknowledgments

The required modifications to the OPTMIS and CNEVAL computational analysis codes were carried out by Mr. Daniel Lesieutre of Nielsen Engineering & Research, Inc., whose help in defining the UAV test problem is gratefully acknowledged. The authors also gratefully acknowledge the support of this work by the Air Force Office of Scientific Research under Air Force STTR Phase I contract FA9550-09-C-0135, monitored by Dr. Fariba Fahroo.

## References

- <sup>1</sup>Gardner, D. R. and Hennigan, G. L., “On Developing a Multifidelity Modeling Algorithm for System-Level Engineering Analysis,” SAND 2003-0399, Feb. 2003.
- <sup>2</sup>Jarrett, J. P., “Multi-Fidelity Gradient-Based Optimization in Turbomachinery Aerodynamic Design,” AIAA 2006-1907, May 2006.
- <sup>3</sup>Wintzer, M., Sturza, P., and Kroo, I., “Conceptual Design of Conventional and Oblique Wing Configurations for Small Supersonic Aircraft,” AIAA 2006-930, Jan. 2006.
- <sup>4</sup>Robinson, T. D., Eldred, M. S., Willcox, K. E., and Haimes, R., “Strategies for Multifidelity Optimization with Variable Dimensional Hierarchical Models,” AIAA 2006-1819, May 2006.
- <sup>5</sup>Robinson, T. D., Willcox, K. E., Eldred, M. S., and Haimes, R., “Multifidelity Optimization for Variable-Complexity Design,” AIAA 2006-7114, Sep. 2006.
- <sup>6</sup>Chang, K. J., Haftka, R. T., Giles, G. L., and Koa, P.-J., “Sensitivity-Based Scaling for Approximating Structural Response,” *J. Aircraft*, Vol. 30, No. 2, Mar.-Apr. 1993, pp. 283-288.
- <sup>7</sup>Hatanaka, K., Obayashi, S., and Jeong, S., “Application of the Variable-Fidelity MDO Tools to a Jet Aircraft Design,” Presented at the 25<sup>th</sup> International Congress of the Aeronautical Sciences, Hamburg, Germany, Sep. 3.-8, 2006.
- <sup>8</sup>Ghoreyshi, M., Badcock, K. J., and Woodgate, M. A., “Integration of Multi-Fidelity Methods for Generating an Aerodynamic Model for Flight Simulation,” AIAA 2008-197, Jan. 2008.
- <sup>9</sup>Forrester, A. I. J. and Keane, A. J., “Recent Advances in Surrogate-Based Optimization,” *Prog. Aero. Sci.*, Vol. 45, Issues 1-3, Jan.-Apr. 2009, pp. 50-79.
- <sup>10</sup>Jones, D., Schonlau, M. and Welch, W., “Efficient Global Optimization of Expensive Black-Box Functions,” *Journal of Global Optimization*, Vol.13, pp. 455-492.

- <sup>11</sup>Singh, G. and Grandhi, R. V., "Mixed-Variable Optimization Strategy Employing Multifidelity Simulation and Surrogate Models," *AIAA Journal*, Vol. 48, No. 1, 2010.
- <sup>12</sup>Gutmann, H.-M., "A Radial Basis Function Method for Global Optimization," *Journal of Global Optimization*, Vol. 19, 2001, pp. 201-227.
- <sup>13</sup>Holmström, K. (2008), An Adaptive Radial Basis Algorithm (ARBF) for Expensive Black-box Global Optimization, *Journal of Global Optimization*, Vol. 41, No. 3, pp. 447-464.
- <sup>14</sup>Floudas, C. A. and Gounaris, C. E., "A Review of Recent Advances in Global Optimization," *Journal of Global Optimization*, Vol. 45, 2009, pp. 3-38.
- <sup>15</sup>Žilinskas, A. "On similarities between two models of global optimization: statistical models and radial basis functions," *Journal of Global Optimization*, Vol. 48, 2010, pp. 173-182.
- <sup>16</sup>Huang, D., Allen, T. T., Notz, W. I., and Miller, R. A., "Sequential Kriging Optimization Using Multiple Fidelity Evaluations," *Structural and Multidisciplinary Optimization*, Vol. 32, No. 5, Nov. 2006, pp. 369-382.
- <sup>17</sup>Schonlau, M., *Computer Experiments and Global Optimization*, Ph.D. Dissertation, University of Waterloo, 1997.
- <sup>18</sup>Lewis, K. and Mistree, F., "The Other Side of Multidisciplinary Design Optimization: Accommodating a Multiobjective, Uncertain and Non-Deterministic World," *Eng. Opt.*, Vol. 31, 1998, pp. 161-189.
- <sup>19</sup>Holden, C. M. E. and Keane, A. J., "Visualization Methodologies in Aircraft Design," AIAA 2004-4449, Sep. 2004.
- <sup>20</sup>Reisenthal, P. H., Love, J. F., Lesieutre, D. J., and Dillenius, M. F. E., "Innovative Fusion of Experiment and Analysis for Missile Design and Flight Simulation," *NATO-RTO Symposium on Innovative Missile Systems*, RTO-MP-AVT-135, Amsterdam, The Netherlands, May 2006.
- <sup>21</sup>Reisenthal, P. H. and Lesieutre, D. J., "Cumulative Metamodeling With Uncertainty Estimation: A New Approach to Risk-Based Optimization of Aerospace Vehicles," NEAR TR 632, Nielsen Engineering & Research, Mountain View, CA, Jul. 2007.
- <sup>22</sup>Kennedy, M. C. and O'Hagan, A., "Predicting the Output of a Complex Computer Code When Fast Approximation are Available," *Biometrika*, Vol. 87, No. 1, 2000, 1-13.
- <sup>23</sup>Schenk, J. R., Huang, D., Zheng, N., and Allen, T. T., "Multiple Fidelity Simulation Optimization of Hospital Performance Under High Consequence Event Scenarios," Proceedings of the 37<sup>th</sup> Winter Simulation Conference, edited by M. E. Kuhl, N. M. Steiger, F. B. Armstrong, and J. A. Joines, 2005.
- <sup>24</sup>Queipo, N. V., Haftka, R. T., Shyy, W., Goel, T., Vaidyanathan, R., and Tucker, P. K., "Surrogate-Based Analysis and Optimization," *Prog. Aero. Sci.*, Vol. 41, 2005, pp. 1-28.
- <sup>25</sup>Reisenthal, P. H., Love, J. F., Lesieutre, D. J., and Childs, R. E., "Cumulative Global Metamodels With Uncertainty -- A Tool for Aerospace Integration," *The Aeronautical Journal*, June 2006, pp. 375-384.
- <sup>26</sup>Huang, D., Allen, T. T., Notz, W. I., and Zheng, N., "Global Optimization of Stochastic Black-Box Systems via Sequential Kriging Meta-Models," *J. Global Opt.*, Vol. 34, No. 3, Mar. 2006, pp. 441-466.
- <sup>27</sup>Press, W., Teukolsky, S., Vetterling, W. and Flannery, B., *Numerical Recipes: The Art of Scientific Computing*, Third Edition, Cambridge University Press, 2007.
- <sup>28</sup>Tseng, S.H., "Bayesian and Semi-Bayesian Regression Applied to Manufacturing Wood Products," Ph.D. Dissertation at The Ohio State University, 2007.
- <sup>29</sup>Lesieutre, D. J., Lesieutre, T. O., and Dillenius, M. F. E., "Planform/Configuration Optimization Program OPTMIS for Arbitrary Cross Section Configurations With Up To Two Fin Sets - Software User's Manual and Software Programmer's Manual," NEAR TR 519, Nielsen Engineering & Research, Apr. 1997.
- <sup>30</sup>Lesieutre, D. J., Dillenius, M. F. E., and Lesieutre, T. O., "Multidisciplinary Design Optimization of Missile Configurations and Fin Planforms for Improved Performance," 7th Symposium on Multidisciplinary Analysis and Optimization, St. Louis, MO, Sep. 1998.
- <sup>31</sup>Dillenius, M. F. E., Lesieutre, D. J., Hegedus, M. C., Perkins, S. C., Jr., Love, J. F., and Lesieutre, T. O., "Engineering-, Intermediate-, and High-Level Aerodynamic Prediction Methods and Applications," *Journal of Spacecraft and Rockets*, Vol. 36, No. 5, Sep.-Oct. 1999, pp. 609-620.
- <sup>32</sup>Rodriguez, J. F., Renaud, J. E., and Watson, L. T., "Convergence of Trust Region Augmented Lagrangian Methods using Variable Fidelity Approximation Data," *Structural Optimization*, Vol. 15, pp. 141-156.
- <sup>33</sup>Reisenthal, P. H., Allen, T. T., Lesieutre, D. J., and Lee, S. H., "Development of Multidisciplinary, Multifidelity Analysis, Integration and Optimization of Aerospace Vehicles," NEAR TR 657, Nielsen Engineering & Research, Santa Clara, CA, 2010.
- <sup>34</sup>Spall, J.C., "Implementation of the Simultaneous Perturbation Algorithm for Stochastic Optimization," *IEEE Transactions on Aerospace and Electronics Systems*, Vol. 34, 817-823.
- <sup>35</sup>Humphrey, D.G. and Wilson, J.R., "A Revised Simplex Search Procedure for Stochastic Simulation Response-Surface Optimization," *INFORMS Journal on Computing*, Vol. 12, 2000, pp. 272-283.
- <sup>36</sup>Gablonsky, J. M. and Kelley, C. T., "A Locally-biased Form of the Direct Algorithm," *Journal of Global Optimization*, Vol. 21, 2001, pp. 27-37.
- <sup>37</sup>Branin, F. H. "Widely Convergent Methods for Finding Multiple Solutions of Simultaneous Nonlinear Equations," *IBM Journal of Research Developments*, 16, 1972, pp. 504-522.
- <sup>38</sup>Eldred, M. S., Giunta, A. A., and Collis, S. S., "Second-Order Corrections for Surrogate-Based Optimization with Model Hierarchies," AIAA 2004-4457, Aug. 2004.